Neural-specific alterations in glycosphingolipid biosynthesis and cell signaling associated with two human ganglioside GM3 synthase deficiency variants

Michelle Dookwah[1], Shannon K. Wagner[1], Mayumi Ishihara[1], Seok-Ho Yu[2], Heidi Ulrichs[3], Michael J. Kulik[3], Nadja Zeltner[3],

Stephen Dalton[3], Kevin A. Strauss[4], Kazuhiro Aoki[1], Richard Steet [ID][2], Michael Tiemeyer [ID][1,*]

[1]Complex Carbohydrate Research Center, University of Georgia, 315 Riverbend Road, Athens, GA 30602, United States
[2]Greenwood Genetic Center, 106 Gregor Mendel Circle, Greenwood, SC 29646, United States
[3]Center for Molecular Medicine, University of Georgia, 325 Riverbend Road, Athens, GA 30602, United States
[4]Clinic for Special Children, 535 Bunker Hill Road, Strasburg, PA 17579, United States

*Corresponding author. Complex Carbohydrate Research Center, University of Georgia, 315 Riverbend Rd., Athens, GA 30602, United States.
E-mail: mtiemeyer@ccrc.uga.edu
†The authors wish it to be known that, in their opinion, the first two authors should be regarded as joint First Authors and that the last three authors should be regarded as joint Corresponding Authors.

GM3 Synthase Deficiency (GM3SD) is a neurodevelopmental disorder resulting from pathogenic variants in the *ST3GAL5* gene, which encodes GM3 synthase, a glycosphingolipid (GSL)-specific sialyltransferase. This enzyme adds a sialic acid to the terminal galactose of lactosylceramide (LacCer) to produce the monosialylated ganglioside GM3. In turn, GM3 is extended by other glycosyltransferases to generate nearly all the complex gangliosides enriched in neural tissue. Pathogenic mechanisms underlying the neural phenotypes associated with GM3SD are unknown. To explore how loss of GM3 impacts neural-specific glycolipid glycosylation and cell signaling, GM3SD patient fibroblasts bearing one of two different *ST3GAL5* variants were reprogrammed to induced pluripotent stem cells (iPSCs) and then differentiated to neural crest cells (NCCs). GM3 and GM3-derived gangliosides were undetectable in cells carrying either variant, while LacCer precursor levels were elevated compared to wildtype (WT). NCCs of both variants synthesized elevated levels of neutral lacto- and globo-series, as well as minor alternatively sialylated GSLs compared to WT. Ceramide profiles were also shifted in GM3SD variant cells. Altered GSL profiles in GM3SD cells were accompanied by dynamic changes in the cell surface proteome, protein O-GlcNAcylation, and receptor tyrosine kinase abundance. GM3SD cells also exhibited increased apoptosis and sensitivity to erlotinib-induced inhibition of epidermal growth factor receptor signaling. Pharmacologic inhibition of O-GlcNAcase rescued baseline and erlotinib-induced apoptosis. Collectively, these findings indicate aberrant cell signaling during differentiation of GM3SD iPSCs and also underscore the challenge of distinguishing between variant effect and genetic background effect on specific phenotypic consequences.

Graphical Abstract
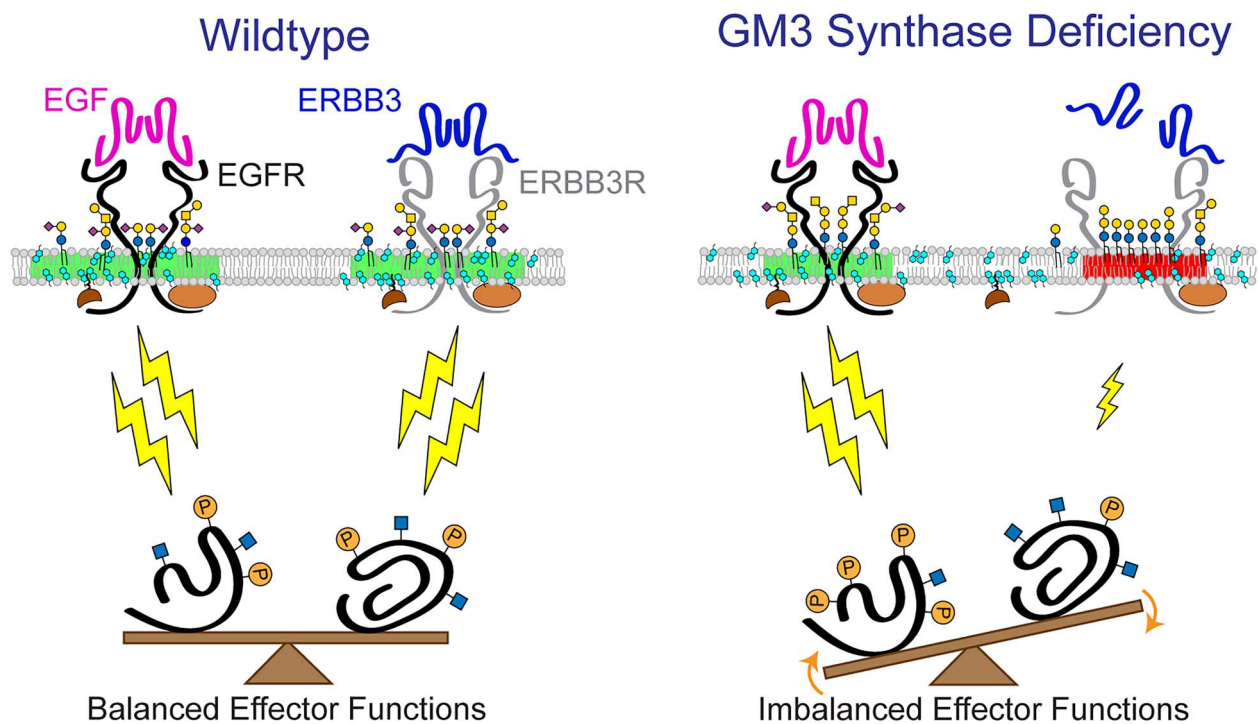
Keywords: GM3 synthase; ST3Gal5; ganglioside; neural crest; signaling

Introduction

GM3 Synthase Deficiency (GM3SD) is an autosomal recessive disorder characterized by infantile-onset epileptic encephalopathy, global developmental delay, postnatal microcephaly, congenital hearing loss, cortical visual impairment, and hyper- and hypopigmented epidermis [1,2]. GM3SD is caused by pathogenic variants in the *ST3GAL5* gene that encodes for the sialyltransferase known as GM3 synthase. ST3GAL5 catalyzes the production of the ganglioside GM3, which is the precursor for all complex a- b-, and c-type ganglioside glycosphingolipids (GSLs) in the human brain (Fig. 1). Gangliosides account for >80% of brain glycans and have been implicated in neural-glial cell interactions, neuronal proliferation and survival, membrane microdomain formation, and cell signaling [3,4]. The significant clinical consequences of GM3SD are not entirely unexpected, in light of the impact of targeted biosynthetic knockouts in mice, and of the accumulated data highlighting *in vitro* functions of gangliosides [5–7]. Nonetheless, the functional impact of altered ganglioside biosynthesis on neural cell differentiation, signaling, and survival in the context of neural cells in culture has not been studied, leaving gaps in our understanding of the neuronal pathogenesis associated with GM3SD.

GM3SD has been associated with several cohorts worldwide, exhibiting allelic diversity based in part on genetic ancestry. Salt & Pepper Syndrome was described as one of the first cohorts of GM3SD, affecting a single family in South Carolina, USA [2,8]. The variant associated with Salt & Pepper Syndrome, *ST3GAL5* c.1063G>A (p.Glu355Lys), encodes for a mutant form of the enzyme lacking any enzymatic activity [9]. A more prevalent variant identified in the Amish population, c.862C > T (p.Arg288Ter), encodes for a truncated and inactive enzyme [9,10]. The Amish variant is estimated to have a carrier frequency of 5%–6% within this population, which translates to approximately 1 in 1200 births [1,11]. The p.Arg288Ter variant has also been reported in French and Pakistani cohorts [12,13]. Additional variant ST3GAL5 mutations have been identified as compound heterozygotes in two Korean siblings (p.Gly201Arg and p.Cys195Ser) and in an African-American Caucasian female (p.Tyr374Cys and p.His389Asp) [14,15]. All of the currently identified and characterized pathogenic ST3GAL5 variants are null for enzymatic activity and/or detectable GM3 and share significant overlap in their clinical presentations [15,16].

To investigate the molecular and neural-specific changes resulting from loss of GM3, we generated induced pluripotent stem cells (iPSCs) from Salt & Pepper (p.Glu355Lys) and Amish cohort (p.Arg288Ter) fibroblasts. These cells were subsequently differentiated toward the neural crest cell (NCC) lineage, and the impact of GM3 synthase deficiency on neural-specific glycosphingolipid biosynthesis and cellular signaling responses was monitored across the differentiation time course. Neural crest was chosen as an initial lineage of study based on skin pigmentation phenotypes described in patients, high homogeneity of the NCC population derived from iPSCs, and the broad impact of neural crest derivatives on somatic function. This investigation identified several common GSL profile alterations in the two variants, including changes in ceramide structures and loss of complex gangliosides. These GSL changes were accompanied by broad fluctuations in multiple cell signaling pathways and an abnormal abundance of several lipid raft-associated cell surface proteins in the two patient lines. The implications of these findings for the neuronal pathogenesis of GM3SD and the limitations that underlie such genotype–phenotype analysis are discussed. These results establish a baseline for the use of patient-derived cells for further investigating the impact of GSL diversity on cell signaling and differentiation in multiple tissue and cell-specific lineages.
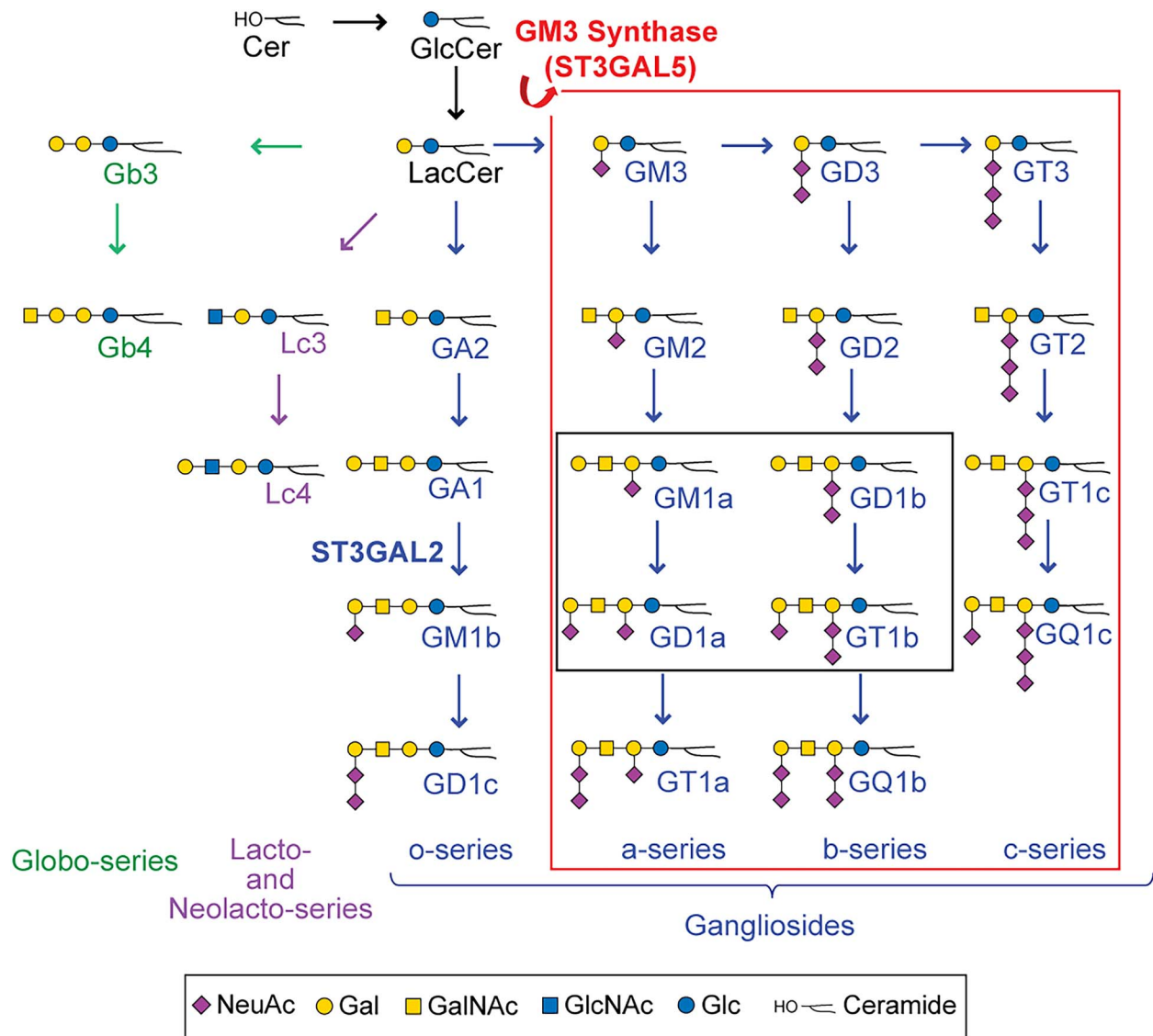
Figure 1. Pathways of human glycosphingolipid biosynthesis. Ceramide (Cer) is glucosylated to form glucosylceramide (GlcCer), which is elongated with a galactose to form lactosylceramide (LacCer). LacCer is the precursor for glycosphingolipid (GSL) elongation into multiple biosynthetic pathways, including the globo-, lacto/neolacto-, and ganglio-series. Sialylation of the GAL residue of LacCer by ST3GAL5 (GM3 synthase) generates the simplest ganglio-series GSL, known as GM3. GM3 is the essential precursor for the production of all a-, b-, and c- series gangliosides (*large box, outlined in red*). Of these gangliosides, four are the most abundant GSLs found in neural tissue, GM1a, GD1a, GD1b and GT1b (*small box, outlined in black*). Graphic representations of GSL monosaccharide residues are consistent with Symbol Nomenclature for Glycans guidelines (SNFG).

Results

GM3 synthase deficiency impacts neural-specific GSL biosynthesis

Characterization of the distribution and abundance of GSLs in WT and GM3SD cell populations by thin-layer chromatography (TLC) and mass spectrometry demonstrates broad similarity as iPSCs, but highly divergent profiles in the differentiated NCC populations. The GSL profiles of iPSCs and NCCs are detectably different by TLC, whether the cells are WT or GM3SD (Fig. 2). WT and GM3SD iPSC GSL profiles are dominated by hexosyl-, lactosyl-, globotriaosyl- and globotetraosylceramide (LacCer, Gb3, and Gb4, respectively). While the analysis presented here cannot distinguish between LacCer and a dihexosylceramide of alternative monosaccharide composition, the only other dihexosylceramide previously described in vertebrate cells is Galα4GalCer, a Gala-series GSL whose expression has been described as a minor

component of the GSL profile of the thymus, kidney, meconium, and myelocytic cancer cells in humans as well as of the heart in chickens [17–23]. Upon differentiation of WT iPSCs to NCCs, LacCer is efficiently shunted toward the production of GM3, along with the more complex gangliosides derived from GM3, such as GD3, GM1, and GD1 (see Fig. 1 for nomenclature). However, differentiation of GM3SD iPSCs results in accumulation of LacCer without production of GM3.

Higher resolution analysis of GSL profiles by NSI-MS^n of their permethylated derivatives validated the lack of GM3 in GM3SD iPSCs and NCCs and the resulting lack of a-, b-, or c-series gangliosides (Figs 3 and 4). By this method, the induced pluripotent stem cell marker SSEA-3 (Gal-extended globotetraosylceramide), itself a GSL, was also detected in WT and GM3SD iPSC GSL profiles. The complex sialylated GSLs of GM3SD NCCs were detected only as o-series gangliosides; these alternatively sialylated GSLs are sialylated on their external Gal residue (GM1b, GD1c, see Fig. 1).
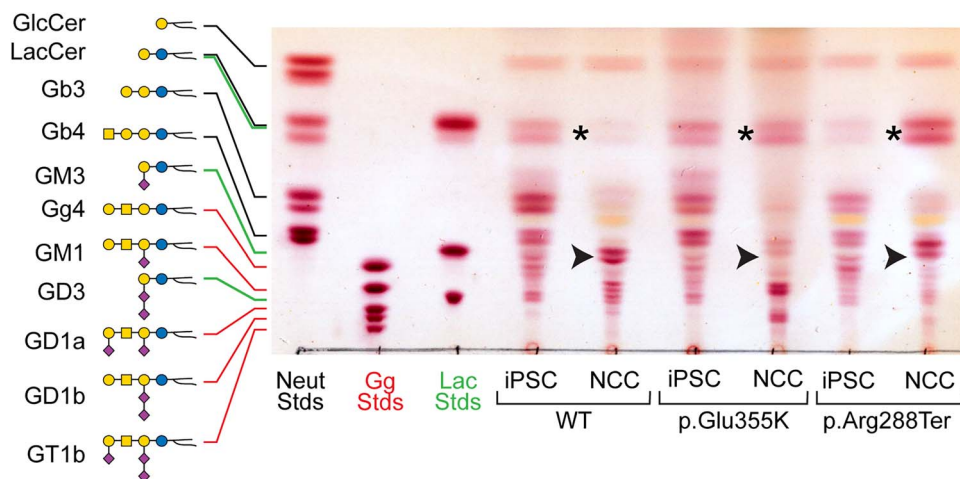
Figure 2. iPSCs and NCCs derived from GM3SD variants fail to produce GM3 and accumulate LacCer. GSLs extracted from WT and GM3SD patient cell types were resolved by TLC and visualized by staining with orcinol reagent. The mobility of three sets of GSL standards are shown for reference (*Neut*, GSLs with neutral cores of increasing length up to globotetraosylceramide, Gb4; *Gg*, GSLs with gangliotetraose cores carrying 0 (asialo, aGM1), 1 (GM), 2 (GD), or 3 (GT) sialic acids; *Lac*, GSLs with a LacCer core carrying 0, 1, or 2 sialic acids). In iPSCs of all three genotypes, the GSL profile is dominated by LacCer and globo-series GSLs. Upon differentiation of WT iPSCs to NCCs, LacCer abundance decreases (*asterisk*) and the appearance of gangliosides is evident, among which GM3 is the most abundant (*arrowhead*). NCCs derived from both GM3SD genotypes retain high levels of LacCer and do not generate GM3.

In the absence of GM3 and GM3-derived GSLs, the GM3SD NCCs retained high levels of LacCer and elevated levels of Gb3 and Gb4 compared to wildtype NCCs.

While the GSL profiles of p.Glu355Lys and p.Arg288Ter iPSCs and NCCs presented similar deficiencies in GM3 and the major GM3-derived GSLs, more subtle differences were detected between the cells derived from the two GM3SD variants. The alternatively sialylated gangliosides GM1b and GD1c were increased in p.Glu355Lys NCCs compared to p.Arg288Ter NCCs (Table 1). Additionally, GSLs with N-acetyl-lactosamine (LacNAc) repeats uncapped by sialic acid at their non-reducing termini were more abundant in p.Arg288Ter NCCs, whereas extended LacNAc structures were more likely to be sialylated in p.Glu355Lys NCCs (Fig. 5, see Supplementary Material, Fig. S1 for validation of the extended LacNAc GSL structures). In general, the major shifts in GSL profiles were conserved across the two GM3SD variants when compared to WT, but p.Glu355Lys NCCs synthesized a higher abundance of alternatively sialylated gangliosides and p.Arg288Ter cells retained greater relative abundance of LacCer and ceramides with higher mass. (Fig. 6A).

GSL ceramide moieties impart physicochemical characteristics that facilitate their incorporation into specialized membrane microdomains referred to as lipid rafts and as detergent resistant membranes [24]. Heterogeneity in GSL ceramides derives from the chemical nature of the sphingosine base and its amide-linked fatty acid. These components can differ based on degree of saturation, hydrocarbon chain length, and presence or absence of a sphingosine hydroxyl group. The heterogeneity of GSL ceramides is well resolved by NSI-MS^n, in which each GSL glycan head group is detected in association with a family of m/z values that reflect lipid differences (Figs 3 and 4). The ratio of longer chain fatty acid-containing ceramides to shorter chain-containing ceramides was higher in the iPSCs of GM3SD patients compared to wild-type; LacCer and globoside Gb4 exhibit this difference particularly well in iPSCs (Figs 3 and 6A). The relative abundance of the longest chain (C24:0 and C26:0) and shortest chain (C16:0) fatty acids did not change appreciably as WT iPSCs differentiated to NCCs, although the relative abundance of intermediate chain lengths (C18:0, C20:0, C22:0, C22:1) was redistributed (Fig. 6B). Similarly,

the relative abundance of the longest and shortest chain fatty acids did not change significantly as p.Arg288Ter iPSCs differentiated to NCCs, although the p.Arg288Ter NCCs (similar to their iPSC precursors) maintained a much higher abundance of the longer chain species than WT NCCs (Fig. 6B). In contrast, the pGlu355Lys NCCs exhibited reduced relative abundance of the longest chain fatty acids compared to their iPSC precursors and to WT and p.Arg288Ter NCCs (Fig. 6B).

GM3 synthase deficiency alters the cell surface proteome

GM3 and several of its precursors and products are components of lipid rafts, plasma membrane microdomains enriched in proteins, frequently GPI-anchored, that participate in multiple cellular functions including adhesion and signaling. We employed a robust cell-surface capture technology (Selective Exo-Enzymatic Labeling or SEEL) to assess whether altered GSL profiles in GM3SD cells impacted the abundance of cell surface proteins, in particular those associated with lipid rafts [24–27]. SEEL installs a biotin moiety onto desialylated N-linked glycans of cell surface glycoproteins, allowing their subsequent high-affinity capture and enrichment for proteomic analysis [28,29]. We applied SEEL to NCCs derived from WT and p.Glu355Lys iPSCs at day 35 of differentiation, captured the resulting biotinylated proteins by immunoprecipitation with anti-biotin antibody, and resolved the precipitated proteins by SDS-PAGE (Fig. 7A).

Subsequent in-gel tryptic digestion and LC-MS/MS analysis identified 120 proteins in WT and 160 proteins in p.Glu355Lys detected at > 10 spectral counts (range 10–460). Gene Ontology (GO) analysis indicated that 96% of the identified proteins were cell surface or cell-surface associated and 4% were nuclear or cytoplasmic. Thus, our SEEL method achieved a stringent enrichment of cell-surface glycoproteins and provided a pool of protein identities for further analysis (Supplementary Material, Table S1). After filtering the total protein identifications to exclude the low-level of contamination with cytoplasmic and nuclear proteins, quantification by spectral counts demonstrated that 73% of the identified cell surface proteins were increased and 27%
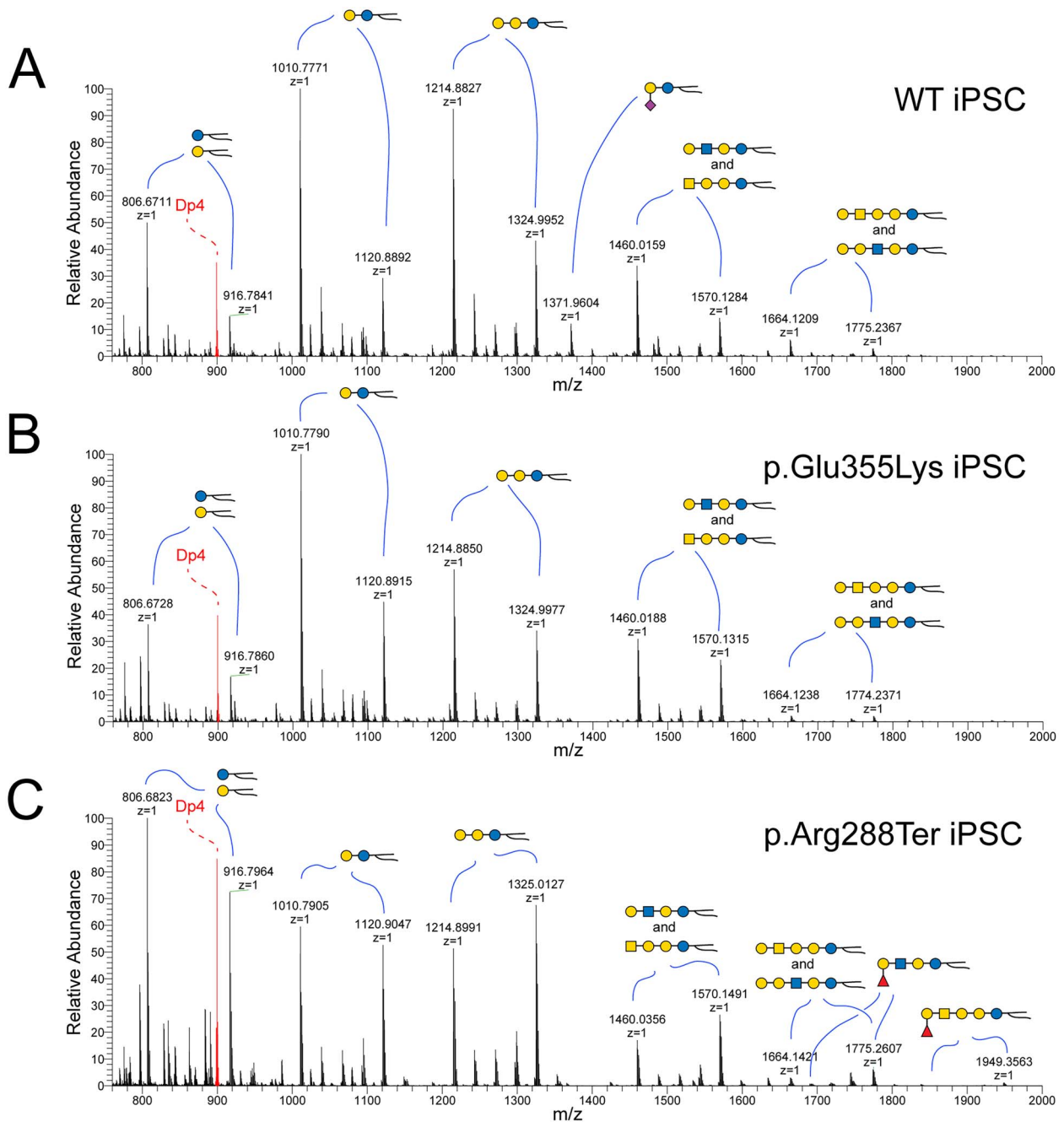
Figure 3. NSI-MS analysis of GSLs extracted from iPSCs detects minor differences in GSL biosynthesis and ceramide compositions. Mass spectra were obtained for permethylated intact GSLs extracted from WT (A), p.Glu355Lys (B), and p.Arg288Ter (C) iPSCs. GSLs with the same glycan headgroup are detected as families of related structures with differing ceramides (*highlighted by curved blue lines*). GM3 is a minor component of the GSL profile of WT iPSCs (*m/z 1372 in A*) but is not detected in either of the GM3SD iPSCs. Both of the GM3SD iPSCs produce a higher relative abundance of longer ceramides; compare the ratio of the LacCer form at m/z 1011 to the form at m/z 1121 across all three iPSCs. The shift in ceramide to higher mass is more pronounced in p.Arg288Ter than in p.Glu355Lys. Internal standard of permethylated maltotetraose (*m/z 885*) is shown in red (*Dp4*).

were decreased in abundance in p.Glu355Lys NCCs compared to WT NCCs.

To assess the impact of GM3SD on the membrane raft and the endocytic pathway proteome, we filtered the identified membrane proteins for GO assignments to the ontologic terms "membrane raft" (GO:0045121) and "endosome" (GO:0005768). Of the total protein identifications, 28% of WT (33 proteins) and 20% of p.Glu355Lys (32 proteins) were annotated with these GO classifications. Among the membrane raft protein identifications, 11 were increased and 3 were decreased in p.Glu355Lys compared

to WT (Fig. 7B). Among the raft-associated proteins, several adhesion receptors (CAD13, CAD15, ICAM1) were detected in WT NCCs that were absent or significantly reduced in p.Glu355Lys NCCs, while other adhesion receptors (DAG1, ITA1, CAD2) were enriched in p.Glu355Lys NCCs compared to WT. Several endocytic receptors, signaling, and adaptor proteins were increased in abundance at the plasma membrane in p.Glu355Lys NCCs in comparison to WT, while a single signaling receptor, a receptor tyrosine kinase (ERBB2) and two peptide hormone processing enzymes (ECE1, LNPEP) were reduced.
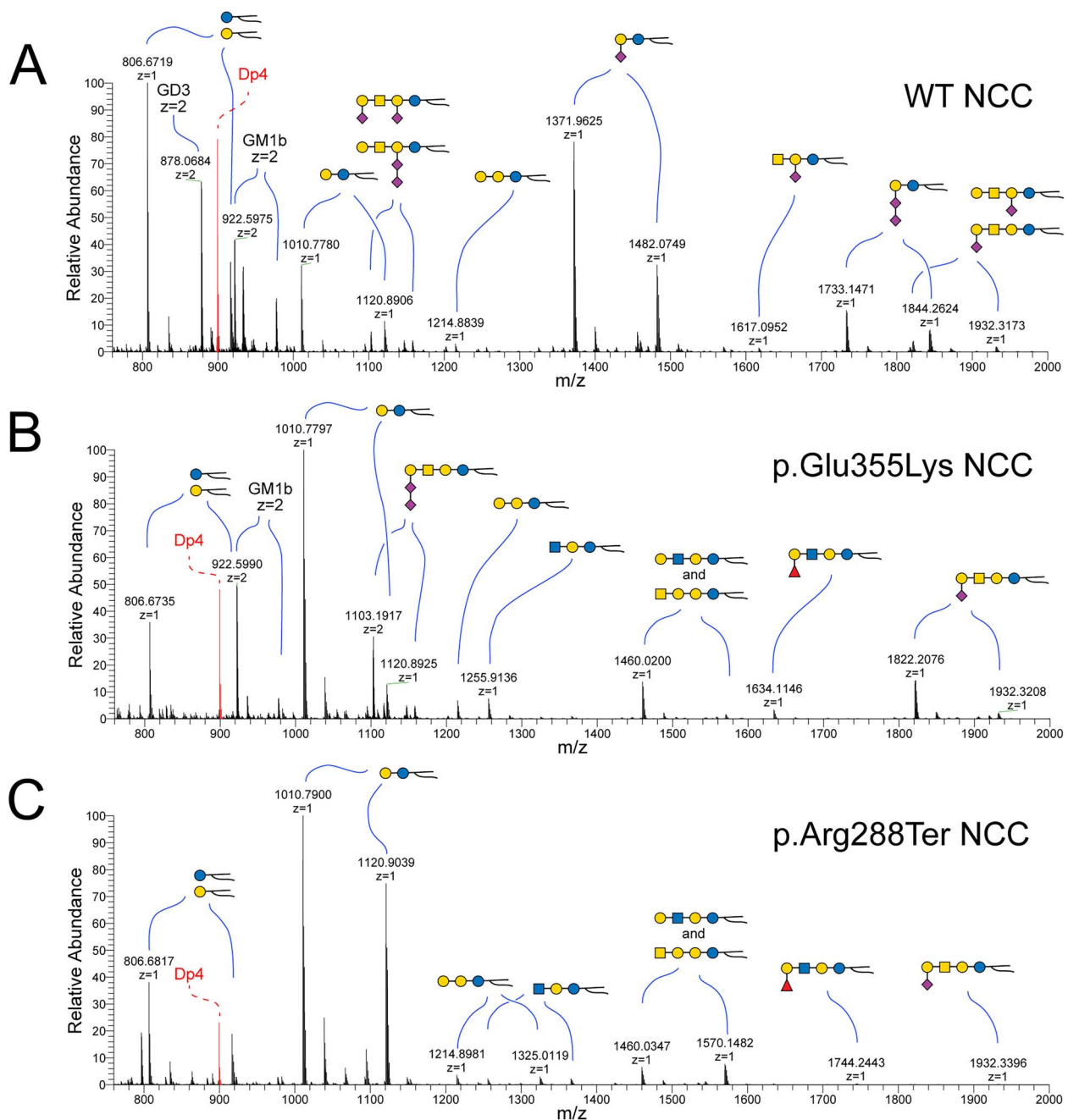
Figure 4. NSI-MS analysis of GSLs extracted from NCCs highlights neural cell-specific alterations in GSL biosynthesis and ceramide compositions. Mass spectra were obtained for permethylated intact GSLs extracted from WT (A), p.Glu355Lys (B), and p.Arg288Ter (C) NCCs. Upon differentiation of WT iPSCs to NCCs, GM3 becomes the most abundant GSL, but is not detectable in GM3SD NCCs. Both populations of GM3SD NCCs retain elevated LacCer (*m/z* 1011–1103). p.Glu355Lys NCCs synthesize alternatively sialylated GSLs, such as GM1b (*m/z* 1822–1932) and GD1c (*m/z* 1103–1159, z = 2), at higher levels than p.Arg288Ter while p.Arg288Ter retains greater abundance of high mass ceramides and p.Glu355Lys exhibits reduced abundance of high mass ceramide compared to WT.

A major component of raft/endosomal membrane trafficking, sortilin (SORT1), was not detected on p.Glu355Lys NCCs following SEEL-based enrichment, but was detected at the surface of WT NCCs. However, western blot analysis of whole cell lysates demonstrated that p.Glu355Lys cells express SORT1 at levels similar to WT NCCs (Supplementary Material, Fig. S2A and Supplementary Material, Table S1). Likewise, NOTCH2, a cell surface receptor important for NCC differentiation into peripheral neurons and other NC-derived cell types, was also not detected following SEEL in p.Glu355Lys NCC cells, but was detected at the surface of WT NCCs, despite being expressed and detected in whole cell lysates (Supplementary Material, Fig. S2B and Supplementary Material,

Table S1). These results indicate that decreased ability to detect these cell surface receptors in GM3SD cells, compared to WT cells, was not due to lack of expression.

GM3 synthase deficiency disrupts protein O-GlcNAcylation, a downstream effector of multiple cell signaling pathways

Protein O-GlcNAcylation is a dynamic modification found on many nuclear and cytoplasmic proteins and is responsive to a broad range of cellular signaling activities, similar to protein phosphorylation. To assess the fidelity of protein O-GlcNAcylation

Table 1. GSL abundance in iPSC and NCC of WT and GM3SD variant cells quantified by mass spectrometry.

GSL[a]	Cell type and Genotype											
	iPSC						NCC					
	Wildtype		p.Glu355Lys		p.Arg288Ter		Wildtype		p.Glu355Lys		p.Arg288Ter	
	%[b]	pmol[c]	%	pmol	%	pmol	%	pmol	%	pmol	%	pmol
LacCer	33.3	277.8	38.5	230.4	29.0	90.1	11.1	35.1	42.4	138.4	75.7	390.4
Gb3	39.1	326.1	26.6	158.9	34.8	108.1	1.0	3.1	2.4	7.9	3.2	16.5
Lc3	—[d]	—	—	—	0.2	0.4	0.4	1.2	2.8	9.0	2.1	10.6
Gb4, Lc4	20.8	173.8	31.5	188.4	21.2	66.0	3.7	11.8	7.8	25.6	16.0	82.3
Fuc-Lc4	1.7	14.1	—	—	14.7	45.8	—	—	2.6	8.5	1.4	7.2
GM3	4.0	33.6	—	—	—	—	46.1	145.6	—	—	—	—
GM2	—	—	—	—	—	—	0.3	1.0	—	—	—	—
GM1a	0.3	2.6	—	—	—	—	1.5	4.6	—	—	—	—
GM1b	0.7	6.0	3.4	20.6	0.1	0.2	13.2	41.8	28.2	92.1	1.6	8.1
GD3	—	—	—	—	—	—	20.2	63.7	—	—	—	—
GD1a	—	—	—	—	—	—	0.5	1.6	—	—	—	—
GD1b	—	—	—	—	—	—	0.3	0.8	—	—	—	—
GD1c	—	—	—	—	—	—	1.8	5.5	13.6	44.5	0.1	0.7

[a]Graphical representations of quantified glycosphingolipids are shown in Fig. 1 along with their abbreviations, except Fuc-Lc4, a terminally fucosylated lactotetraosylceramide (see Figs 3 and 4). [b]GSL relative abundance, denoted "%," is given as the percent that each individual GSL contributes to the total lipid profile for each cell type/genotype. [c]GSL amount, denoted "pmol," is given as pmol/1×10^6 cells. [d]Double dash denotes GSL not detected.
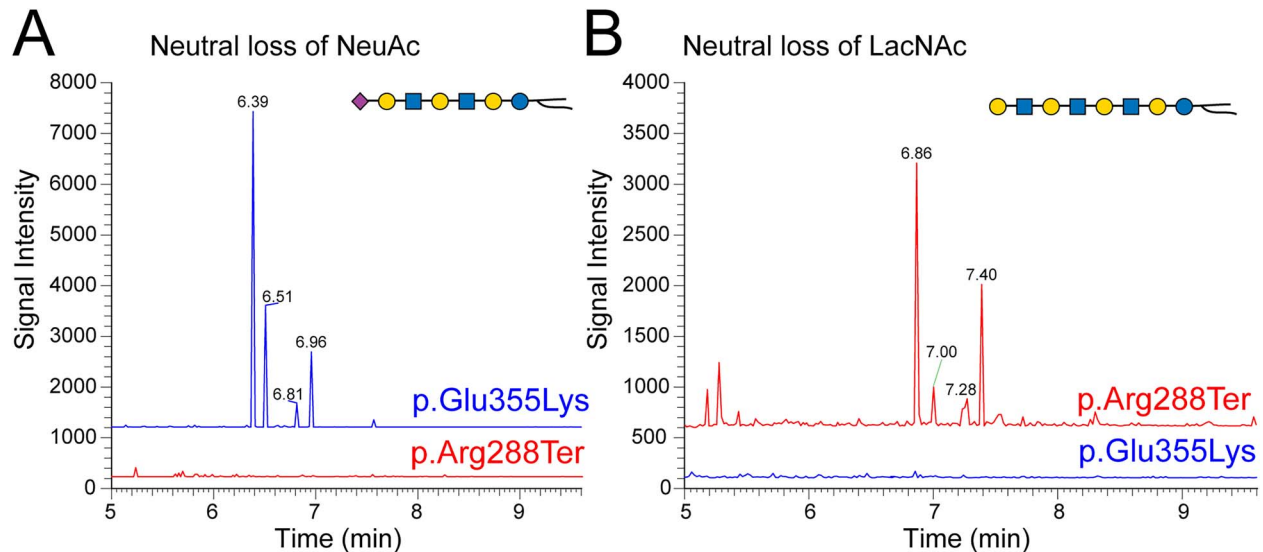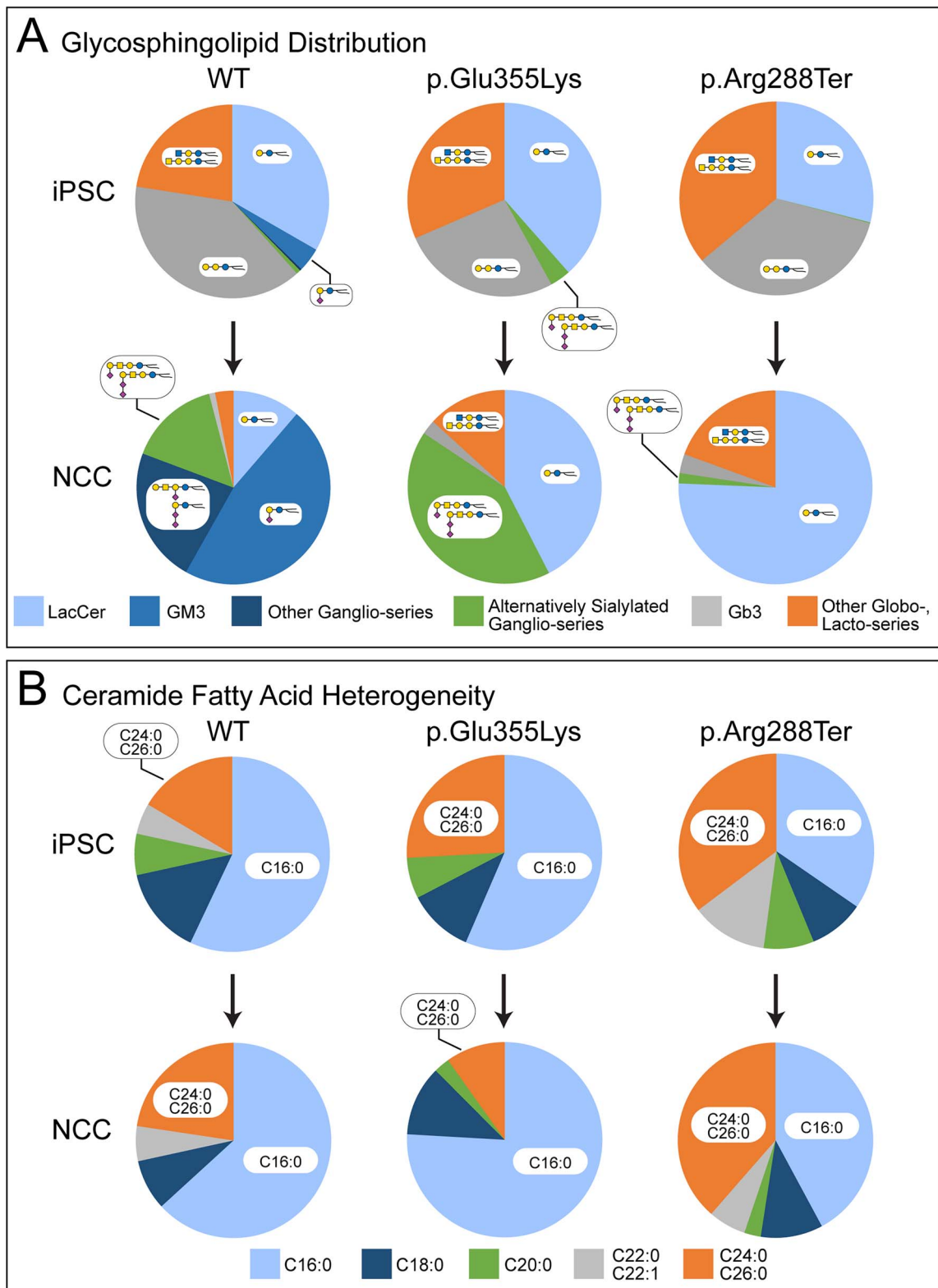

Figure 5. Unique GSL changes in GM3SD variants. The results of Total ion monitoring workflows (TIM-chromatograms) were filtered for neutral loss of NeuAc or LacNAc. (A) Filtering for loss of NeuAc demonstrates that GSLs with extended LacNAc repeats capped with sialic acid are detected at higher abundance in p.Glu355Lys NCCs than in p.Arg288Ter NCCs. (B) Filtering for loss of LacNAc disaccharide demonstrates that non-sialylated forms of GSLs with LacNAc repeats are more abundant in p.Arg288Ter than in p.Glu355Lys NCCs. MS2 fragmentation profiles support the structural assignments at the indicated TIM detection times (Supplementary Material, Fig. S1). These less abundant unique GSLs, like the more abundant GSLs in NCCs, also show greater enrichment of higher mass ceramides in p.Arg288Ter than in p.Glu355Lys (e.g. compare the ratio of peaks at 6.96/6.39 in A to 7.40/6.86 in B).

in the absence of complex gangliosides, we probed whole cell lysates for the presence of O-GlcNAc in iPSCs and NCCs derived from WT and GM3SD cells (Fig. 8). For both WT and GM3SD cells, the abundance of O-GlcNAc modified proteins increased upon differentiation of iPSCs to NCCS (Fig. 8 and Supplementary Material, Fig. S3). For WT cells, the increase in O-GlcNAcylation in NCCs reached statistical significance ($P < 0.02$) compared to iPSCs. For p.Glu355Lys and p.Arg288Ter cells, O-GlcNAcylation levels were also increased in NCCs, but the variance in the detected levels was too great to reach statistical significance. Nonetheless, the fold-increase in O-GlcNAcylation in NCCs relative to iPSCs for each separate differentiation was comparable for WT, p.Glu355Lys, and p.Arg288Ter: 3.4 ± 0.9 in WT, 4.1 ± 1.1 in p.Glu355Lys, and 3.6 ± 0.8 in p.Arg288Ter cells ($p > 0.05$ for pairwise comparisons, $n = 3$

independent differentiations for each cell type). The apparent molecular weight profile of proteins detectable by western blot of one-dimensional SDS-PAGE gels was also different in iPSCs compared to NCCs, but was not qualitatively altered across genotypes (Supplementary Material, Fig. S3).

Receptor tyrosine kinases are impacted by GM3 synthase deficiency

To assess whether GM3SD broadly impacts cell surface signaling events that lie upstream of protein O-GlcNAcylation, we used an array-based approach to query receptor tyrosine kinase (RTK) activity in whole-cell lysates prepared from WT and p.Glu355Lys iPSCs and NCCs at day 19 of differentiation. This method takes advantage of immobilized antibodies to capture RTKs from cell
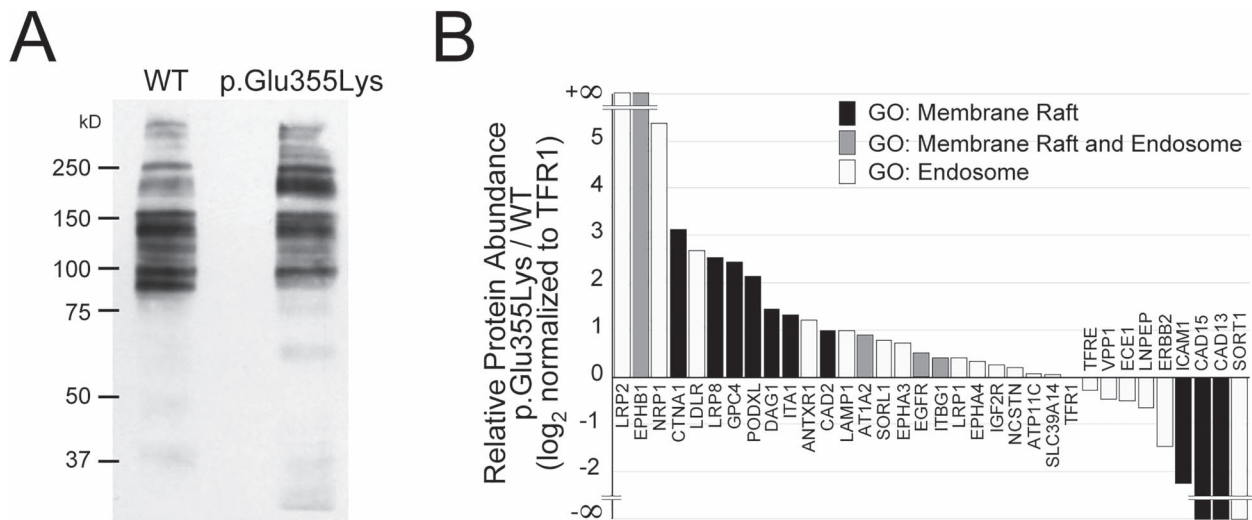
Figure 6. Summary of GSL and ceramide fatty acid abundance changes in iPSCs and NCCs of wildtype and GM3SD variants. The relative abundance of the major GSL types detected in iPSCs and NCCs demonstrate relatively minor differences in iPSCs but more significant changes upon differentiation to NCCs. (A) As WT iPSCs differentiate to NCCs, decreases in the relative abundance of LacCer, Gb3, and other Globo-, and Lacto-series GSLs are mirrored by increases in GM3 and other Ganglio-series GSLs. Differentiation of GM3SD variant iPSCs to NCCs is accompanied by maintenance of LacCer as a major GSL and by complete lack of Ganglio-series GSLs that depend on ST3GAL5 activity. (B) The relative abundance of the ceramide fatty acids of LacCer were quantified. Although their iPSC fatty acid profiles are quite different, as WT and p.Arg288Ter cells differentiate to NCCs, relatively minor changes are observed, especially comparing the shortest (C16:0) to the longest (C24:0, C26:0) fatty acids. The fatty acid profile of p.Glu355Lys iPSCs is similar to WT iPSCs but as the p.Glu355Lys cells differentiate to NCCs, the relative abundance of the shortest chains (C16:0) expands at the expense of the longest chain fatty acids (C24:0, C26:0).

Figure 7. Cell surface protein abundance is altered in GM3SD cells. NCCs differentiated from WT or p.Glu355Lys iPSCs were subjected to selective-exoenzymatic labeling (SEEL) to install a biotin moiety specifically on cell surface glycoproteins. (A) Labeled proteins were resolved by SDS-PAGE and probed by western blot with anti-biotin antibody, revealing the presence of changes in the abundance of membrane proteins. (B) Gel-resolved proteins were harvested by in-gel digestion with trypsin and identified by LC–MS/MS. Identified proteins assigned to the indicated Gene Ontology (GO) categories were compared to assess the integrity of lipid rafts and the endosomal pathway. (Supplementary Material, Table S1).
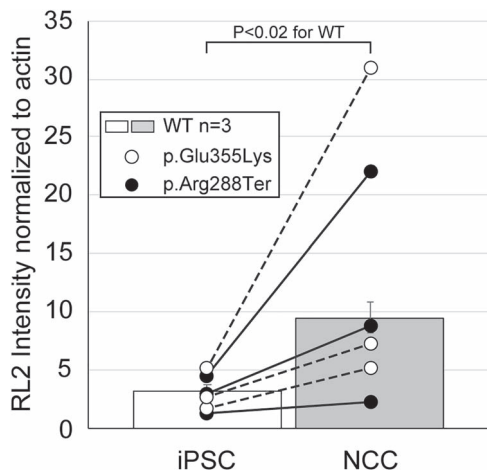

Figure 8. Protein O-GlcNAcylation increases upon differentiation of iPSCs to NCCs. Whole cell lysates from WT and GM3SD cells were resolved by SDS-PAGE, blotted, and probed with RL2, a monoclonal antibody that recognizes proteins modified by O-GlcNAc, and quantified by densitometry. Individual differentiation experiments for GM3SD cells are shown connected by a dashed or solid line (n = 3 independent differentiations). GM3SD cell values are plotted on top of bars that represent the mean ± SEM for WT cells (n = 3 independent differentiations). The statistical significance of the difference (P-value from pairwise T-test) are presented above the bars for comparison of WT iPSCs and WT NCCs O-GlcNAcylation.

lysates for subsequent detection of the phosphorylation status of the captured RTKs following incubation of the blots with a pan-phosphotyrosine antibody. The major RTKs detected in WT and GM3SD iPSC lysates were EGFR, ERBB3, INSR, and IGF2, each of which were detected at approximately equal intensity comparing WT to GM3SD (Supplementary Material, Fig. S4A). Upon differentiation to NCCs, ERBB3 intensity was increased, while EGFR, INSR, and IGF1 intensities were not substantially modified (Supplementary Material, Fig. S4B). EGFR was similar to WT in GM3SD NCC lysates, while INSR and IGF-1 intensities were slightly decreased. Most striking, however, was the loss of ERBB3 detection in GM3SD NCC lysates. This array-based method reports

changes in the overall phosphorylation of the represented RTKs but does not resolve whether the changes relate to altered activity or differences in protein expression. Therefore, we independently assessed the steady-state levels of EGFR and ERBB3 receptors during NCC differentiation.

EGFR (also known as ERBB1) possesses a binding domain in its extracellular region that interacts with gangliosides, in particular GM3 [30]. EGFR also forms a heterodimer with ERBB3, thought to be a poor kinase by itself, to facilitate signaling in response to heregulin/neuregulin binding [31–33]. To understand whether the differences in ERBB3 detected on the array blots resulted from altered phosphorylation or from differential protein expression/stability, we probed cell lysates with phosphorylation-independent antibodies for EGFR and ERBB3 across the time course of differentiation from iPSCs to NCCs (Supplementary Material, Fig. S4C–E). As WT iPSCs differentiate toward NCCs, they exhibit a reproducible and complementary expression profile in which EGFR increases early in differentiation compared to iPSCs and then decreases upon completion of the differentiation process (Fig. 9A). ERBB3 mirrors the EGFR profile, exhibiting an early decrease in abundance that transforms into increased abundance in NCCs compared to iPSCs. The evolving time course of EGFR and ErbB3 expression during differentiation from iPSCs to NCCs was highly reproducible across biological replicates, with the maximum variability occurring during times of greatest change in receptor expression (d0–d15 of differentiation).

We assessed EGFR and ERBB3 expression in p.Glu355Lys and p.Arg288Ter cells across the same differentiation course from iPSCs to NCCs and compared the GM3SD cells to WT (Fig. 9B, C and Table 2). Both the p.Glu355Lys and p.Arg288Ter cell populations exhibit significant variation from WT across all timepoints of differentiation. For EGFR, significant differences across the three cell populations were detected during mid (d11–22) and late (d3–32) stages of differentiation (ANOVA p < 0.01 and p < 0.001, respectively). Pairwise comparisons demonstrated that EGFR expression in p.Glu355Lys was significantly decreased compared to WT at late stages (p < 0.05), while expression in p.Arg288Ter was significantly increased in mid and late stages (p < 0.01 and p < 0.05, respectively). For ERBB3, significant
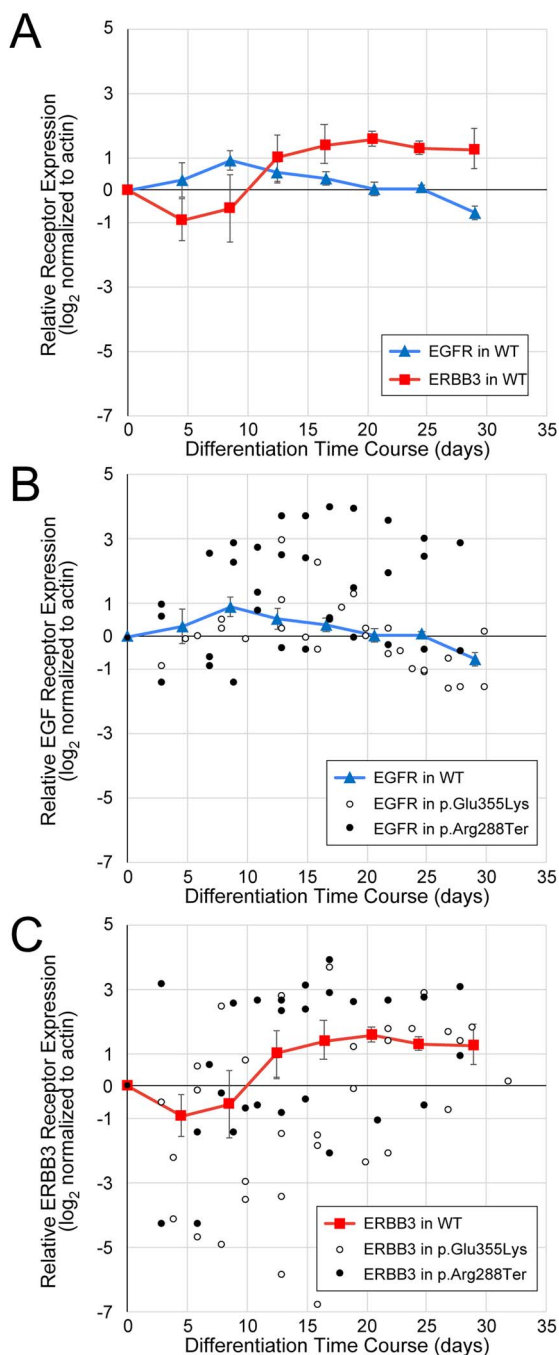
Figure 9. Dynamics of EGFR and ERBB3 expression during neural crest differentiation. Protein-specific, not phospho-specific, antibodies against EGFR and ERBB3 were used to quantify receptor expression in WT and GM3SD cells across full time courses of differentiation from iPSCs to NCCs (n = 3 independent differentiations for each cell type). (A) EGFR and ERBB3 expression mirror each other as WT iPSCs differentiate to NCCs. For simplicity of presentation and to provide a baseline reference for comparison with GM3SD cells, WT values were combined into bins that span 4 days of differentiation (mean ± SEM, n = 4–6 determinations for each bin, total of 30 data points for each receptor). (B) Individual time points for EGFR abundance are plotted for three independent differentiations of GM3SD cells (n = 27 data points for p.Glu355Lys, n = 32 data points for p.Arg288Ter); WT EGFR profile is reproduced from panel A for reference. (C) Individual time points for ERBB3 abundance are plotted for three independent differentiations of GM3SD cells (n = 37 data points for p.Glu355Lys, n = 32 data points for p.Arg228Ter); WT ERBB3 profile is reproduced from panel A for reference. Table 2 presents P-values for ANOVA and pairwise T-tests of ERBB3 and EGFR expression differences between WT and GM3SD cells during differentiation.

differences were also detected in GM3SD cells compared to WT, especially at mid stages of differentiation (ANOVA p < 0.05). Pairwise comparisons demonstrated that ERBB3 expression in p.Glu355Lys was significantly reduced at this stage (p < 0.05) but p.Arg288Ter was not significantly different from WT. Pairwise comparisons of EGFR and ERBB3 expression between p.Glu355Lys and p.Arg288Ter further highlight subtle differences between the two GM3SD cell populations, with EGFR expression more highly impacted in p.Arg288Ter and ERBB3 more impacted in p.Glu355Lys cells. Furthermore, the deviation detected for EGFR and ERBB3 in the p.Glu355Lys cells is consistent with the RTK blot, namely ERBB3 was affected more than EGFR at d19 of differentiation (see Supplementary Material, Fig. S4).

EGFR/ERBB3-dependent cell survival is compromised in GM3 synthase deficiency cells

EGFR and ERBB3 signaling support cell survival [34,35]. Fluctuations in these signaling pathways may therefore lead to decreased survival of differentiating cells. We investigated the impact of altered abundance of these essential RTKs on cell survival by assessing the appearance of cleaved caspase3, an apoptotic effector, in differentiating GM3SD cells (Fig. 10). While cleaved caspase3 was detected in WT and both GM3SD iPSCs, it decreased to undetectable levels in WT cells by the mid-point of differentiation to NCCs (Fig. 10A). In contrast, levels of cleaved caspase3 remained detectable through d13 in differentiating p.Glu355Lys cells (Fig. 10B) and through d17 in p.Arg288Ter cells (Fig. 10C). This result suggested that GM3SD cells are more prone to programmed cell death during differentiation to NCCs, a phenotype that may relate to altered EGFR/ERBB3 abundance.

In order to test the hypothesis that altered ganglioside and glycolipid biosynthesis increases the likelihood of cell death, we stressed the EGFR/ERBB3 signaling pathway by exposing cells to erlotinib, a pharmacologic inhibitor of EGFR signaling, at the mid-point (d11–d13) of iPSC differentiation to NCCs [36]. We observed that treatment with erlotinib resulted in significant detachment of presumably apoptotic cells from the surface of the tissue culture well. GM3SD cells dissociated from the surface of the culture well to a much greater extent than WT cells and significant levels of cleaved caspase3 were detected within the floating cell population (Supplementary Material, Fig. S5A). Exposure of WT cells to 100 μM erlotinib for 24–48 h resulted in a consistent and time-dependent increase in the ratio of cleaved to full-length caspase3, although the increase did not achieve statistical significance (Table 3 and Fig. 10D). In both populations of GM3SD cells, cleaved caspase3 levels were markedly more variable than in WT with or without erlotinib treatment. Upon erlotinib challenge, p.Glu355Lys and p.Arg288Ter cells exhibited statistically significant increases in cleaved caspase3 at one or more timepoints whether the GM3SD cells were compared to erlotinib-treated or vehicle-treated WT cells (Table 3 and Fig. 10D). Collectively, these findings demonstrate an increased sensitivity of the GM3SD cells to erlotinib during NCC differentiation, a phenotype that may relate to unregulated expression/abundance of RTKs such as EGFR/ERBB3 during critical stages of differentiation.

Pharmacologic inhibition of O-GlcNAcase rescues viability of GM3 synthase deficiency cells

Protein O-GlcNAcylation is responsive to many cellular response pathways and has been proposed to serve as a signal integrator that regulates downstream effectors [37]. The increase in O-GlcNAcylation that we detected in WT NCCs compared to iPSCs and the indication that absolute levels of protein O-GlcNAcylation

Table 2. EGFR and ERBB3 expression in iPSC and NCC of WT and GM3SD variant cells.

Differentiation Time (Days)	Receptor Expression (log$_2$ normalized to actin)			ANOVA P-value	Pairwise T-Test P-Value		
	Wildtype Mean ± SEM (n)	p.Glu355Lys Mean ± SEM (n)	p.Arg288Ter Mean ± SEM (n)		p.Glu355Lys vs. Wildtype	p.Arg288Ter vs. Wildtype	p.Glu355Lys vs. p.Arg288Ter
EGFR							
Early (3–10)	0.61 ± 0.36 (6)	−0.10 ± 0.20 (6)	0.49 ± 0.58 (9)	0.5806	0.0572	0.8778	0.2170
Mid (11–22)	0.18 ± 0.18 (12)	0.63 ± 0.31 (12)	1.73 ± 0.38 (18)	0.0046	0.1112	0.0018	0.0235
Late (23–32)	−0.37 ± 0.18 (9)	−1.06 ± 0.20 (9)	1.44 ± 0.79 (5)	0.0005	0.0101	0.0130	0.0009
ERBB3							
Early (3–10)	−0.77 ± 0.62 (7)	−1.78 ± 0.75 (11)	−0.69 ± 0.87 (9)	0.5269	0.3586	0.9489	0.3543
Mid (11–22)	1.39 ± 0.28 (12)	−0.60 ± 0.90 (16)	1.47 ± 0.46 (16)	0.0429	0.0370	0.4473	0.0245
Late (23–32)	1.24 ± 0.48 (7)	2.68 ± 0.79 (10)	1.51 ± 0.46 (7)	0.2691	0.0945	0.7029	0.1378
				P > 0.05	P < 0.05	P < 0.01	P < 0.001

are more variable in GM3SD cells than in WT (see Fig. 8), suggested that pharmacologic manipulation of O-GlcNAcylation might attenuate the impact of altered EGFR/ERBB3 expression in GM3SD cells. To test this hypothesis, we treated WT and p.Arg288Ter cells with thiamet G, a specific inhibitor of the hexosaminidase (O-GlcNAcase) responsible for removing O-GlcNAc from nuclear and cytoplasmic proteins, with or without co-treatment with erlotinib (Fig. 10E and Supplementary Material, Fig. S5B). Since p.Arg288Ter cells exhibited greater cleaved caspase than p.Glu355Lys cells during unperturbed differentiation (compare Fig. 10B and C) and following 48 h treatment with erlotinib (Fig. 10D), we chose to treat this population of cells as a more stringent test of the hypothesis. While thiamet G treatment tended to decrease cleaved caspase3 in WT cells, the decreases were not significant when comparing thiamet G treatment to vehicle alone, erlotinib alone, or to thiamet G + erlotinib treatment at 24 or 48 h of exposure (Table 4). Dual treatment of p.Arg288Ter cells with erlotinib and thiamet G resulted in cleaved caspase3 levels that were reduced compared to erlotinib alone (compare Fig. 10D and E). Although trending upwards from 24 to 48 h of dual exposure in p.Arg288Ter cells, the cleaved caspase ratio was statistically indistinguishable from erlotinib treated WT cells at 24 and 48 h of exposure, indicating that increased O-GlcNAcylation rescued erlotinib-induced apoptosis of GM3SD cells (Fig. 10E and Table 4).

Discussion

Here we report the characterization of two different GM3SD patient iPSC-derived neural crest cell lines and demonstrate the involvement of several signaling pathways not previously recognized in the context of this human disorder. Importantly, these studies establish deficiency of numerous complex gangliosides and accumulation of different globosides within the GM3SD NCC lineage. Moreover, the glycolipid profile changes occur at the same stage of differentiation at which the key alterations in signaling and receptor expression are observed, suggesting a causal relationship. The implication of these findings toward the pathophysiology of GM3SD, and the key limitations of this work, are discussed below.

Complex gangliosides are essential components of the extracellular leaflet of the plasma membrane of neural cells. Subsets of these GSLs, including GM3, preferentially partition into lipid microdomains that are also enriched in cell-signaling receptors and adhesion molecules [25,26]. Therefore, mutations in the biosynthetic enzymes responsible for generating GSLs would be expected to impart significant pathology. Surprisingly, however, the first reports of a mouse knockout of St3gal5 described a relatively normal animal capable of surviving and reproducing [6]. Subsequent analysis demonstrated more subtle defects such as cochlear neuronal cell death, reduced male fertility, altered insulin receptor signaling, and skewed inflammatory responses [6, 38–41]. The relatively mild nature of the mouse St3gal5 knockout phenotype has been proposed to result from the ability of that organism to efficiently sialylate extended GSL cores on external Gal residues to generate o-series GSLs (Fig. 1). These gangliosides, which we refer to here as alternatively sialylated gangliosides, may be capable of at least partially compensating for loss of the a-, b-, and c-series gangliosides [42]. An alternate hypothesis has been proposed by Russo and colleagues that suggests the accumulation of globosides in certain cells and organisms can be a primary driver of pathogenesis [43,44]. Our previously published work on p.Glu355Lys patient fibroblasts demonstrated that human fibroblasts do not possess a robust capacity to produce significant amounts of o-series, alternatively sialylated gangliosides [8]. It was thought that in the absence of this alternative GSL biosynthetic capacity, patients with GM3SD manifest significant neurologic complications that are not currently well modeled in the mouse.

Consistent with our previous report on p.Glu355Lys fibroblasts, GSL profiles of iPSCs and NCCs from both GM3SD variants were devoid of GM3 and GM3-derived GSLs [8,10]. Other than loss of GM3, the GSL profile of GM3SD iPSCs was strikingly similar to WT, suggesting that GM3SD should be expected to have a minimal impact on the maintenance of pluripotency and, perhaps, of neural stem cell populations in developing or mature brains. However, the value of modeling human disease in iPSC-derived cell populations became apparent upon differentiation of GM3SD cells to NCC, as neural-specific and variant-specific changes in
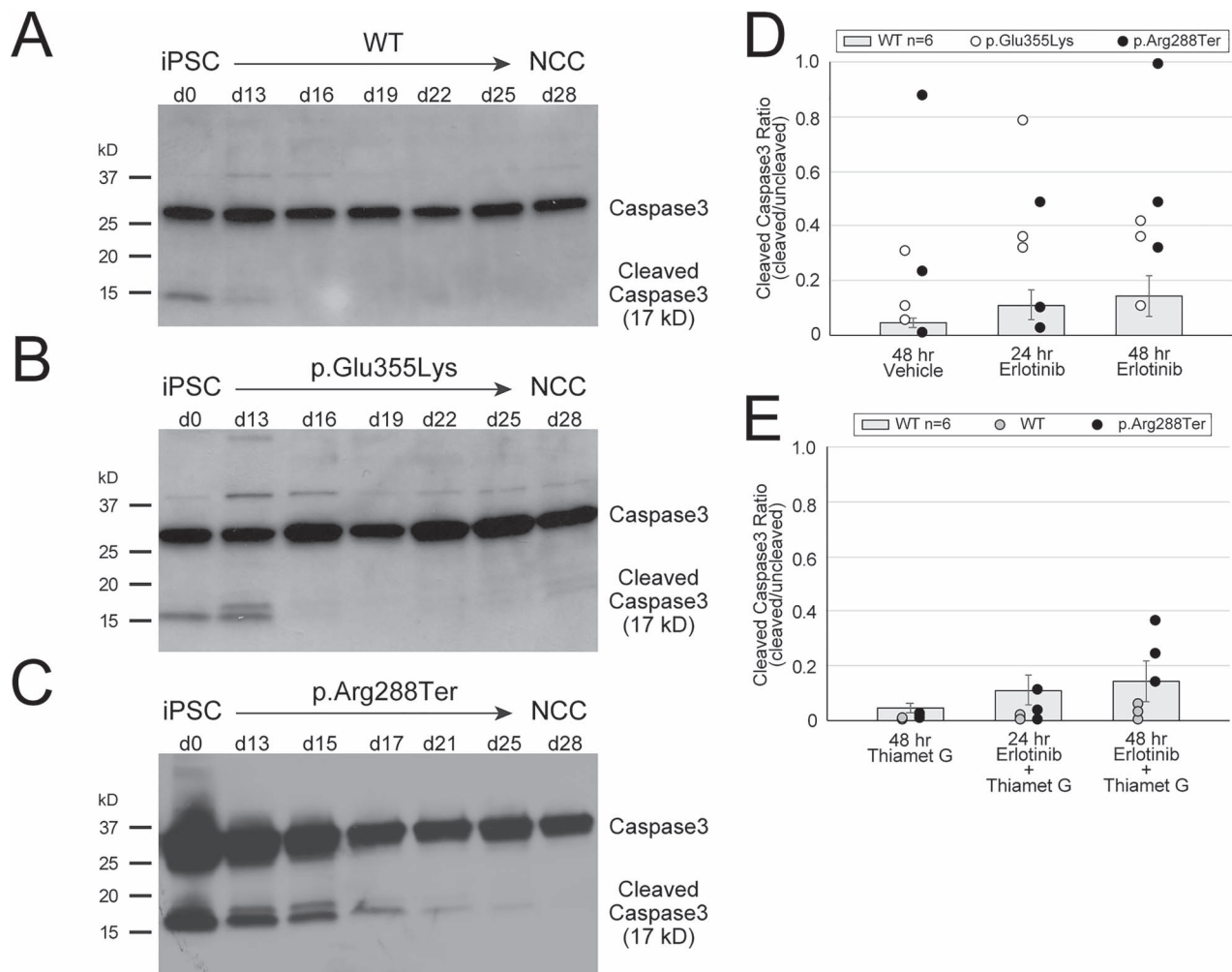
Figure 10. GM3SD apoptosis during differentiation is enhanced by altered EGFR signaling and rescued by increased protein O-GlcNAcylation. Apoptosis, reported by the abundance of cleaved Caspase3, is detectable in WT and GM3SD iPSC cultures (A, B, C) at day 0 (*d0*). As WT cells differentiate to NCCs (A), cleaved Caspase3 is barely detectable at the midpoint of the differentiation course (*d13*), whereas it remains at or above iPSC levels in p.Glu355Lys (B) and p.Arg288Ter (C) cells at the same time point and beyond. (D) GM3SD cells are more sensitive to erlotinib treatment than WT cells (GM3SD data points present 3 independent differentiations and are plotted on top of bars that present mean ± SEM for n = 6 independent differentiations of WT cells treated similarly). Table 3 presents P-values for ANOVA and pairwise T-tests of differences in cleaved Caspase3 between WT and GM3SD cells treated with erlotinib. (E) Thiamet G treatment, which enhances protein O-GlcNAcylation by inhibition of O-GlcNAcase, decreases Caspase3 cleavage in WT and p.Arg288Ter GM3SD cells. (WT and p.Arg288Ter data points present 3 independent differentiations and are plotted on top of bars that present mean ± SEM for n = 6 independent differentiations of WT cells treated with vehicle or erlotinib alone, reproduced from panel D). Table 4 presents P-values for pairwise T-tests of differences in cleaved Caspase3 between WT and GM3SD cells treated with erlotinib and Thiamet G.

GSL profiles became evident. In GM3SD NCCs, the absence of a-, b-, and c-series gangliosides was associated with large increases in LacCer, the precursor to GM3, and parallel increases in globo- and lacto-series GSLs compared to WT. Other neural-specific changes in GM3SD cells included enhanced production of the alternatively sialylated gangliosides GM1b and GD1c in p.Glu355Lys and greater retention of LacCer in p.Arg288Ter cells compared to each other and to WT. Thus, a hallmark of human GM3SD is the retention and partial rerouting of LacCer into other biosynthetic pathways. The extent to which the clinical phenotypes of GM3SD arise from elevated LacCer or globo-series GSLs, reduced complex ganglioside biosynthesis, or a combination of both remains unknown, but the iPSCs and NCCs we describe here provide a useful platform to investigate the impact of GSL imbalance at the cellular level.

An important caveat for the studies reported here is that our observations are based on iPSCs derived from a single representative of each of the p.Glu355Lys and p.Arg288Ter variants. Neither the p.Glu355Lys or p.Arg288Ter variant polypeptides have

been detected as endogenously expressed proteins in human tissues or derived cells. However, both proteins are produced when expressed as epitope-tagged forms in HEK cells but lack measurable transferase activity [9]. Thus, while both variants are functionally null, it remains to be determined whether mRNA produced from an endogenous variant *ST3GAL5* gene locus can lead to the translation of a stable enzyme variant. The molecular nature of the two ST3GAL5 protein variants fails to suggest an obvious mechanism by which either might differentially impact alternative sialylation. It will be essential to continuously evaluate individual-to-individual variation in patient-derived cell types as more patient samples become available [15,16]. Notably, significant individual-to-individual variation in plasma GSL abundance and ceramide diversity was not previously detected across unrelated individuals in the p.Arg288Ter GM3SD patient population [45]. Nonetheless, it is likely that differences in genetic or epigenetic background of the two different patient lines studied here contribute to biochemical diversity; GSLs have been suggested

Table 3. Cleaved Caspase3 in WT and GM3SD variant cells at mid-differentiation with and without EGFR inhibition by erlotinib.

Treatment	Cleaved Caspase3 Ratio (cleaved/uncleaved)[a]			ANOVA P-value	Pairwise T-test P-value					
	WT[b]	p.E355K	p.R288*		p.E355K vs. WT	p.R288* vs. WT	p.E355 vs. p.R288*	WT Erlotinib vs. WT Vehicle	p.E355K Erlotinib vs. WT Vehicle	p.R288* Erlotinib vs. WT Vehicle
Vehicle	0.026 ± 0.013	0.151 ± 0.076	0.368 ± 0.261	0.1506	0.0251	0.0868	0.4701	—	—	—
24 h Erlotinib	0.115 ± 0.053	0.498 ± 0.143	0.040 ± 0.027	0.0093	0.0080	0.3826	0.0344	0.1343	0.0008	0.5805
48 h Erlotinib	0.158 ± 0.070	0.291 ± 0.095	0.593 ± 0.202	0.0637	0.3054	0.0179	0.2484	0.0958	0.0047	0.0019
				P > 0.05	P < 0.05	P < 0.01	P < 0.001			

[a]Cleaved Caspase3 Ratios are given as the mean ± SEM of 3–6 independent differentiations. [b]Cell types are abbreviated as WT (wildtype), p.E355K (p.Glu355Lys), and p.R288* (p.Arg288Ter).

to drive a high degree of functional heterogeneity within dermal fibroblast lines [43]. If such a mechanism is extended to the iPSC and iPSC-derived cell types, this GSL-driven heterogeneity may partially explain the striking variability we observed in receptor expression and other phenotypic readouts in variant cell populations.

The relevance of iPSC-derived cell types for understanding biochemical and physiologic responses to disease-causing gene variants in patient tissues should be evaluated on a disease-by-disease basis. Previously published results characterized the fatty acid distribution of the ceramides associated with LacCer in wildtype (non-affected human subjects) and GM3SD (p.Arg288Ter homozygous subjects) patient populations [45]. Analysis of the fatty acid distributions of the LacCer ceramide moieties detected in iPSCs and NCCs of WT and p.Arg288Ter revealed striking similarities between patient plasma, patient-derived iPSCs, and differentiated NCCs (Supplementary Material, Fig. S6). While WT and GM3SD cells exhibited distinct fatty acid profiles, both were consistent with the plasma profiles of wildtype and p.Arg288Ter patients, respectively. Thus, despite cellular reprogramming and subsequent differentiation to NCCs, derived cells grown in tissue culture media exhibited ceramide fatty acid profiles consistent with the plasma profiles of a population of patients with the same ST3GAL5 genotype. The conservation of ceramide heterogeneity in iPSCs and derived cell types adds support for the validity of modeling GSL-mediated cellular responses in the patient-derived cells we report here.

SEEL-based capture of cell surface glycoproteins in WT and p.Glu355Lys NCCs identified both enrichment and loss of membrane raft associated proteins whose GO functions indicate roles in cell adhesion, cell signaling, axon pathfinding, neurogenesis, nervous system development, and cell migration. Neuropathological data at cellular resolution is not yet available for GM3SD brain tissue, making it difficult to associate specific cellular and developmental processes (neuroblast/neural stem cell proliferation and migration, axonal/dendritic outgrowth, neuropil expansion, myelination, etc.) with altered ganglioside biosynthesis. However, delayed neurologic development and reduced cranial growth are characteristic of GM3SD and point to likely impairments in the types of functions associated with the proteins whose presence we detected as altered at the cell surface of GM3SD cells [1]. Minimally, these changes are consistent with material changes in the physicochemical nature of the plasma membrane and in membrane subdomains relevant for signaling and adhesion.

Although the molecular mechanisms by which specific GSLs contribute to the self-associative generation or stabilization of signaling microdomains remain elusive, direct interactions between GM3 and RTKs such as EGFR have been functionally and structurally demonstrated [30, 46–49]. Weak, potentially disruptive binding between EGFR or other RTKs and the alternatively sialylated GSLs produced by GM3SD cells may significantly impact the efficiency of receptor partition into signaling domains, the efficacy of their signaling activity, or the extent of their residence time at the cell surface (Fig. 11). As pluripotent WT cells proceed down any particular differentiation pathway (e.g. to NCCs), receptor signaling activates and inhibits various cellular effector functions to appropriately tune or balance responses toward achieving a particular endpoint. Phosphorylation and O-GlcNAcylation of effector proteins are frequently responsible for driving these responses (Fig. 11A).

While protein phosphorylation is well recognized as a regulatory post-translational modification, many nuclear and

Table 4. Cleaved Caspase3 in WT and GM3SD variant cells at mid-differentiation in presence of EGFR (erlotinib) and O-GlcNAcase (thiamet G) inhibition.

Treatment	Cleaved Caspase3 Ratio (cleaved/uncleaved)[a]		Pairwise T-test P-value			
	Wildtype	p.Arg288Ter	Wildtype Thiamet G *vs.* Wildtype Vehicle[b]	Wildtype Erlotinib + Thiamet G *vs.* Wildtype Thiamet G	Wildtype Erlotinib[b] *vs.* Wildtype Erlotinib + Thiamet G	p.Arg288Ter Erlotinib + Thiamet G *vs.* Wildtype Erlotinib[b]
Vehicle [b]	0.026 ± 0.013	0.368 ± 0.261	0.2455	—	—	—
Thiamet G alone	0.002 ± 0.001	0.012 ± 0.005	—	—	—	—
24 h Erlotinib + Thiamet G	0.016 ± 0.007	0.048 ± 0.031	—	0.1101	0.2462	0.4326
48 h Erlotinib + Thiamet G	0.028 ± 0.016	0.245 ± 0.064	—	0.1911	0.2531	0.4569
			P > 0.05			

[a]Cleaved Caspase3 Ratios are given as the mean ± SEM of 3–6 independent differentiations. [b]Values for these Cleaved Caspase3 Ratios taken from Table 3.

cytoplasmic proteins are also modified by the addition of O-linked GlcNAc at Ser/Thr residues in response to a broad range of cellular signaling activities. O-GlcNAcylation is dynamically driven by the cellular micro-environment, nutrient availability, cell stress, cell cycle, growth factors and associated developmental events, as well as other signals [37]. Thus, like phosphorylation, the profile of O-GlcNAcylated proteins reflects the integration of signals through multiple pathways. We demonstrated that protein O-GlcNAcylation increased as WT and GM3SD iPSCs differentiated to NCCs but the amount of O-GlcNAc modification was much more broadly distributed in GM3SD cells. By pharmacologically enhancing O-GlcNAcylation with thiamet G, cleaved caspase3 levels were significantly reduced in WT and GM3SD cells in the presence or absence of erlotinib [50,51]. This intervention suggests that, despite broad variation in the expression of primary signaling receptors like EGFR and ERBB3, modulation of downstream effectors can rescue the impact of altered GSL biosynthesis on basic cellular processes in neural lineages (Fig. 11B).

Our results demonstrate the importance of investigating glycosylation changes associated with mutations in glycan biosynthetic enzymes in appropriate cell types. We previously described collateral changes in N-linked and O-linked glycosylation of glycoproteins expressed by p.Glu355Lys fibroblasts [8]. Such collateral changes are of interest because ST3GAL5 does not act on glycans linked to proteins; it is absolutely GSL-specific. Thus, the matrix of regulatory processes that control cellular glycosylation are responsive to changes that span glycan classes. This phenomenon has also recently been demonstrated in glyco-engineered human cell lines [52]. The results presented here provide the first characterization of GSL biosynthetic, cell signaling, and cellular survival changes associated with human-derived neural cells in GM3SD. We have identified global changes in GSL biosynthesis that correspond to substantial alterations in cell signaling and residence of glycoproteins at the plasma membrane. We have also identified more subtle changes that may provide differential characteristics capable of distinguishing GM3SD variants. As additional cohorts of GM3SD patients are identified and become available for analysis at the cellular level, the results reported here will provide a framework for assessing functional differences that may provide insight into clinical phenotypes. The iPSC platform

we have characterized also presents opportunities to assess the potency of molecular and small-molecule therapeutic interventions that might resolve these cellular phenotypes and impact broader glycomic and pathophysiologic consequences associated with GM3SD.

Materials and methods
Generation of induced pluripotent stem cells

Wild-type iPSC lines hiPSK3 and hiC3 were, respectively, acquired from Steve Duncan, University of Wisconsin, or generated from ATCC CRL-1509 human fibroblasts [53]. Generation of p.Glu355Lys iPSCs (from ST3GAL5 c.1063G>A (p.Glu355Lys) patient fibroblasts) and p.Arg288Ter iPSCs (from ST3GAL5 c.862C>T (p.Arg288Ter) patient fibroblasts) was performed using the CytoTune-iPS Sendai Reprogramming Kit (Invitrogen, # A13780) and the CytoTune-iPS 2.0 Sendai Reprogramming Kit (ThermoFisher, # A16517), respectively, using the manufacturer's conditions and as described previously [54]. The p.Glu355Lys donor was a 13 year old male of African-American descent and the p.Arg288Ter donor was a 12 year old male and a member of the Amish community. A single iPSC clone was generated for the p.Glu355Lys variant and 3 independent clones were generated for the p.Arg288Ter variant. Each subclone was passaged at least 10 times to ensure removal of residual reprogramming virus before further characterization. Loss of virus was monitored by staining with anti-Sendai virus antibody (Invitrogen, cat #14649482).

iPSC clones were initially tested for pluripotency by assessing expression of pluripotency markers Oct4 (Cell Signaling, # C30A3), SSEA3/4 (Santa Cruz, # sc-21704), and Sox2 (R&D, # MAB2018), and by inducing differentiation into neuroectodermal cells as previously described [55]. For neuroectoderm differentiation, cells were fixed and stained for PAX6 (Biolegend, # 901301/B201255) and DAPI at day 4 following plating and exhibited efficient differentiation into the neuroectodermal lineage (Supplementary Material, Fig. S7). All iPSCs were tested for mycoplasma every 2 weeks. The three independent iPSC clones derived from p.Arg288Ter donor fibroblasts and the single clone derived from p, Glu355Lys donor fibroblasts exhibited equivalent differentiation potential and growth characteristics (Supplementary Material, Figs S7–9). In the absence of any observable
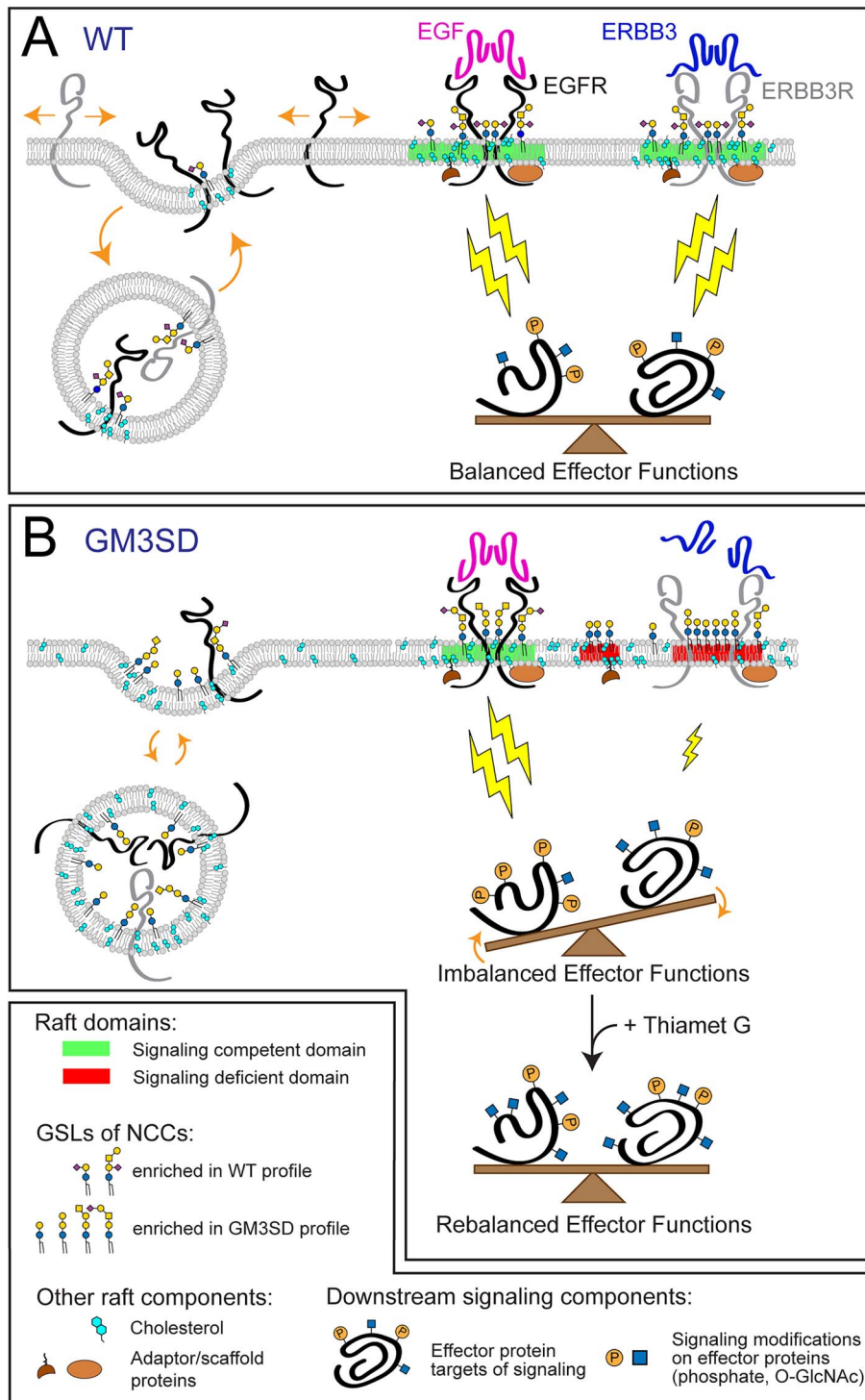
Figure 11. GSL composition impacts lipid rafts and cell signaling in GM3SD. Cell membrane lipid composition influences many cellular functions. Therefore, altered GSL biosynthesis might be expected to *two* have pleiotropic consequences, some of which are illustrated here in relation to their possible contribution to the cellular pathology associated with GM3SD. Cell surface signaling receptors are regulated by their migration in-and-out of membrane signaling domains and by the balance of their internalization/reinsertion kinetics. In WT and GM3SD cells, lipid raft characteristics reflect the physicochemical properties of the GSLs, phospholipids, and sterols that constitute the plasma membrane. (A) When cells are able to synthesize GM3 and its subsequent end-products, functional lipid rafts (*shaded regions of membrane, shown in green*) facilitate the association of signaling receptors and adaptor/scaffold proteins to appropriately stimulate downstream effectors (*lightning bolts*). Membrane recycling also buffers signaling responses by internalizing surface receptors and shuttling additional signaling capacity from intracellular storage. Effector functions are balanced by appropriate receptor activation, membrane insertion, and physical interactions within signaling domains. (B) In the absence of GM3, GSL compositions are shifted toward greater abundance of neutral lipids and toward the appearance of alternatively sialylated species. The characteristics of the resulting dysfunctional lipid rafts (*two shaded regions of membrane on the right, shown in red*) reflect deficiencies in the ability of these GSLs to interact with receptors and with other raft components. Consequently, increased or decreased signaling through modified rafts may generate imbalanced effector functions that impact cellular responses. Pharmacologic interventions, such as increasing protein O-GlcNAcylation (thiamet G), may establish an alternative balance in effector functions that counters otherwise deleterious downstream processes.

differences in the growth and differentiation characteristics of the three p.Arg288Ter clones, the p.Arg288Ter.2.1a was selected for the glycolipidomic and biochemical analyses described here (Supplementary Material, Fig. S7).

Neural crest differentiation of iPSCs

Patient and WT iPSCs were differentiated to neural crest cells (NCCs) according to a previously published protocol [54]. Cells exhibited NCC morphology between day 7–10 of differentiation. By Day 15, cells tested positive by immunohistochemistry for NC markers HNK1 (Sigma Aldrich, # C6680) and p75 (Advanced Targeting Systems, # AB-N07), and negative for iPSC markers Oct4, SSEA3/4, and Sox2 (Supplementary Figs S7–9). Cells were collected for analysis by scraping and centrifugation at $200 \times g$ for 5 min. Supernatants were removed by aspiration and the resulting pellets were stored frozen until analysis. Successful differentiation of WT and GM3SD variant iPSCs to NCCs was monitored by endpoint analysis for the acquisition of NCC markers and loss of pluripotency markers by immunofluorescence as described below. Marker assessment was performed over multiple independent differentiations and repeated upon thaw of each new aliquot of an iPSC line [54].

Immunofluorescence staining

Antibodies and dilutions were as follows: Anti-HNK-1 antibody (Sigma Aldrich, Monoclonal Anti-HNK-1/N-CAM (CD57), # C6680), 1:200 dilution in 5% donkey serum prepared in 0.2% Triton X-100 in PBS (PBS-T); Anti-Sox2 antibody (R&D, # MAB2018), 1:200 dilution in 5% donkey serum in PBS-T; Anti-Oct4 antibody (Santa Cruz, # sc-8628), 1:200 dilution in 5% donkey serum in PBS-T; Anti-Pax6 antibody (Santa Cruz, # sc-81649), 1:200 dilution in 5% donkey serum prepared in 0.05% Tween-20 in PBS (PBS-T); Anti-SSEA3/4 antibody (Santa Cruz, # sc-21704), 1:200 dilution in 5% donkey serum in PBS-T; Anti-p75 antibody (Advanced Targeting Systems, # AB-N07), 1:100 dilution in PBS-T. All antibodies were incubated overnight at 4°C. Immunofluorescent images were captured using an Olympus Fluoview FV1000 laser confocal microscope or a LionheartFX (BioTek) fluorescence microscope.

Extraction, preparation, and analysis of GSLs by TLC and mass spectrometry

iPSCs or iPSC-derived NCCs were homogenized and extracted with organic solvents to precipitate proteins and recover GSLs as described previously [56]. Initial analyses of WT and GM3SD GSLs were performed by TLC using the solvent system C/M/W (60:40:10) for GSL mixtures. Orcinol–H_2SO_4, resorcinol, Dittmer-Lester, and Ninhydrin reagents were used for the detection of sugar, sialic acid, phosphate, and primary amine groups, respectively. Nanospray ionization mass spectrometry (NSI-MS) was performed on permethylated glycolipids by direct infusion into a linear ion trap mass spectrometer (Orbi-LTQ; ThermoFisher Scientific) using a nanospray source [56–59]. The instrument was tuned with a mixture of permethylated standard neutral or ganglioside GSLs. For fragmentation by collision-induced dissociation (CID) in MS/MS and MS^n, a normalized collision energy of 30%–35% was used. Detection, structural identification, and quantification of individual glycolipids were accomplished using full MS, total ion mapping (TIM), and neutral loss scan (NL scan) functionalities of the Xcalibur software package version 2.0 (ThermoFisher Scientific) as previously described [45,56]. Quantification of the amount of each permethylated GSL (as pmol/1×10^6 cells) was achieved by referencing GSL peak heights in full MS spectra to the peak height of a known quantity of a permethylated glycan

standard, maltotetraose (Dp4), which was spiked into the sample prior to MS, as previously described [45,60]. Most glycolipid components were identified as singly, doubly, and triply charged, sodiated species (M + Na) in positive mode. Peaks for all charge states were summed for quantification. Graphic representations of GSL monosaccharide residues are consistent with the Symbol Nomenclature For Glycans (SNFG) as adopted by the glycomics and glycobiology communities [61]. Glycomics data and metadata were obtained and are presented in accordance with MIRAGE standards and the Athens Guidelines [62,63]. All raw mass spectrometric data, both glycomic and proteomic, were deposited at GlycoPost, Accession GPST000363 [64].

Selective Exo-Enzymatic labeling of cell surface glycoproteins

Selective Exo-Enzymatic Labeling (SEEL) installs a biotin moiety onto the N-linked glycans of cell-surface glycoproteins, allowing their subsequent high-affinity capture and enrichment for proteomic analysis [28,29]. SEEL and subsequent proteomic analysis of tagged proteins were conducted on WT and p.Glu355Lys iPSCs and NCCs according to previously described methods [29]. Recombinant rat α-(2,6)-sialyltransferase (ST6GAL1) was prepared as previously described [65]. Biotinylated CMP-sialic acid was synthesized as described previously according to [29]. For labeling of cell-surface glycoproteins, approximately 9x10^7 NCCs from WT and p.Glu355Lys lines were dissociated from the cell culture dish by manual trituration in Dulbecco's phosphate-buffered saline (DPBS). The cells were pelleted and resuspended in serum-free DMEM with 42 μg/ml ST6Gal1, 34 μM CMP-Sia-C5-biotin, 13.3 μg/ml BSA, 13.3 μg/ml alkaline phosphatase and 2 μl (in 50% glycerol) *Arthrobacter ureafaciens* (AU) neuraminidase. After a 2 h SEEL labeling incubation at 37°C, cells were lysed in RIPA buffer and biotinylated proteins were captured by immunoprecipitation from 1 mg total lysate protein using anti-biotin antibody. Precipitated proteins were resolved by SDS-PAGE, visualized by silver stain, and processed as previously described [29]. The resulting peptides and glycopeptides were analyzed by LC-MS/MS using a Lumos Tribrid mass spectrometer (ThermoFisher). Proteins identified by peptides detected at <10 spectral matches (PSMs) were excluded from analysis, as were peptides identified as nuclear or cytosolic by GO annotation (Supplementary Material, Table S1). Spectral counts for cell surface and secreted proteins that met threshold criteria were normalized to the number of spectral counts detected for human transferrin receptor in WT and p.Glu355Lys IPs.

Identification of receptor tyrosine kinases in WT and GM3SD cells

Protein was harvested from WT and p.Glu355Lys iPSC and NCC lysates (d19 of differentiation) using the manufacturer's Receptor Tyrosine Kinase (RTK) array protocol in Lysis buffer 17 (R&D Systems, # ARY001B). RTK arrays were blocked for 1 h at room temperature in Array Buffer 1 (manufacturer's protocol). An amount of protein (300 μg) from each cell lysate was diluted in Array Buffer 1 to a volume of 1.5 ml and added to the blocked RTK arrays. Arrays were then incubated with gentle rocking overnight at 4°C. The arrays were then washed 3× with 1× Wash Buffer (manufacturer's protocol) and subsequently probed with HRP-conjugated pan-phosphotyrosine antibody diluted in Array Buffer 2 (manufacturer's protocol). Following incubation with gentle rocking for 2 h at room temperature, the blots were washed with Wash Buffer and RTK capture/phosphorylation was detected by chemiluminescence using the manufacturer's protocols.

Western blot analysis

Antibodies for detection of cell surface proteins by western blot of cell lysates were used as provided and were from the following sources: anti-ERBBB3 (Cell Signaling, HER3/ERBB3, D22C5 XP Rabbit mAb, # 12708) at 1:1000 dilution with detection by goat anti-mouse secondary at 1:2500 dilution; anti-EGFR (Santa Cruz, EGFR A-10, # sc-373 746) at 1:1000 dilution with detection by goat anti-mouse secondary at 1:2500 dilution; anti-caspase 3 (Santa Cruz, caspase-3 Antibody 31A1067, # sc-56 053) at 1:1000 dilution with detection by goat anti-mouse secondary at 1:2500 dilution; anti-sortilin (BD Biosciences, Neurotensin Receptor 3 antibody, # 612100) at 1:1000 dilution with detection by goat anti-mouse secondary at 1:2500 dilution; anti-NOTCH2 (DSHB, NOTCH2 C651.6DbHN) at 1:500 dilution with detection by goat anti-rat secondary at 1:3000 dilution; anti-β-actin (Santa Cruz, Actin Antibody 2Q1055, # Sc-58 673) at 1:5000 dilution with detection by goat anti-mouse secondary at 1:2500 dilution. O-GlcNAcylation of proteins in cell lysates was detected by western blot with anti-O-GlcNAc monoclonal antibody RL-2 (Enzo Life Sciences, ALX-804-11-R100) at 1:1000 dilution with detection by goat anti-mouse secondary at 1:10000. Actin was detected in parallel with O-GlcNAc by incubation with anti-β-actin (Cell Signaling Technology, Actin Antibody 13E5, #4790) at 1:5000 with detection by goat anti-rabbit secondary at 1:10 000.

Protein concentrations in lysates were measured by BCA assay and aliquots containing 25 μg were reduced, alkylated, resolved by SDS-PAGE, and transferred to PVDF membranes for probing with primary antibodies. Primary antibody binding was detected by HRP-conjugated secondary antibodies and chemiluminescence. Densitometric quantification was performed with ImageJ Software. For developmental time courses that assessed the change in abundance of receptors across differentiation from iPSC to NCC, signal intensities for receptor proteins were normalized to ß-actin (loading control) and then expressed as $\log_2$-fold changes relative to the normalized signal intensity detected in iPSC (d0 of differentiation).

Pharmacologic inhibition of EGFR signaling by erlotinib and of O-GlcNAcase by thiamet-G

WT and p.Glu355Lys iPSCs were differentiated to NCCs for 10 days as previously described [54]. Beginning at d10, vehicle (2% DMSO final) or erlotinib in vehicle (100 μM final concentration in media) or thiamet-G in vehicle with or without erlotinib (10 μM thiamet-G ± 100 μM erlotinib final concentration in media) was added to a media change and the cells were incubated for 24 or 48 additional hours prior to harvest for analysis. At harvest timepoints, the media was removed from the wells and centrifuged to collect floating cells. Adherent cells were also scraped and pelleted for collection. Adherent and floating cells were lysed prior to analysis by BCA assay and analyzed separately by western blot for the relative abundance of cleaved and uncleaved caspase 3.

Statistical analysis

Western blot analyses were performed on cells harvested at indicated time points from between 3–6 independent differentiation courses. Multiple parametric tests were utilized to assess the statistical significance of the resulting data. One-way ANOVA was used to identify significant changes across the three cell populations: WT, p.Glu355Lys, and p.Arg288Ter. Z-scores were calculated and subjected to Z-test to assess the distribution of WT and GM3SD population data for EGFR and ERBB3 expression, where the large number of independent replicates allowed for reasonable estimation of the standard deviation of the entire population. Pairwise T-tests were also used to assess the similarity of one population compared to another for specific features, especially for assessing pharmacologic effects on smaller sample sets. For all three tests, a P-value less than or equal to 0.05 was considered indicative of a significant difference between the tested populations. The results of pairwise T-tests and Z-tests identified the same population differences as significant; for simplicity of presentation, only the pairwise T-tests are presented for direct comparisons. In tables and graphs, population means are reported ± standard error of the mean. For the analysis of EGFR and ERBB3 expression, immunoblot band intensities for each receptor were normalized to actin intensity in order to control for loading variability and then presented as $\log_2$ of the ratio for each timepoint relative to day 0 of the differentiation course. For the analysis of cleaved Caspase3, the ratio of the immunoblot intensity associated with the cleavage product at 17kD was divided by the ratio of the intensity associated with the intact protein at 34kD detected in the same lane; normalization to actin was not performed since the ratios are independent of sample load.

Supplementary data

Supplementary data is available at *HMG Journal* online.

Conflict of interest statement. None declared.

References

1. Bowser LE, Young M, Wenger OK. *et al.* Recessive GM3 synthase deficiency: natural history, biochemistry, and therapeutic frontier. *Mol Genet Metab* 2019;**126**:475–88.
2. Saul R, Wilkes G, Stevenson R. In: *Proc. Greenwood Genet. Ctr*, 1983;**2**:6–9.
3. Schnaar RL, Gerardy-Schahn R, Hildebrandt H. Sialic acids in the brain: gangliosides and polysialic acid in nervous system development, stability, disease, and regeneration. *Physiol Rev* 2014;**94**:461–518.
4. Sipione S, Monyror J, Galleguillos D. *et al.* Gangliosides in the brain: physiology, pathophysiology and therapeutic applications. *Front Neurosci* 2020;**14**:572965.
5. Schnaar RL. Gangliosides of the vertebrate nervous system. *J Mol Biol* 2016;**428**:3325–36.

6. Yamashita T, Hashiramoto A, Haluzik M. *et al.* Enhanced insulin sensitivity in mice lacking ganglioside GM3. *Proc Natl Acad Sci* 2003;**100**:3445–9.

7. Lloyd KO, Furukawa K. Biosynthesis and functions of gangliosides: recent advances. *Glycoconj J* 1998;**15**:627–36.

8. Boccuto L, Aoki K, Flanagan-Steet H. *et al.* A mutation in a ganglioside biosynthetic enzyme, ST3GAL5, results in salt & pepper syndrome, a neurocutaneous disorder with altered glycolipid and glycoprotein glycosylation. *Hum Mol Genet* 2013;**23**:418–33.

9. Indellicato R, Parini R, Domenighini R. *et al.* Total loss of GM3 synthase activity by a normally processed enzyme in a novel variant and in all ST3GAL5 variants reported to cause a distinct congenital disorder of glycosylation. *Glycobiology* 2019;**29**:229–41.

10. Simpson MA, Cross H, Proukakis C. *et al.* Infantile-onset symptomatic epilepsy syndrome caused by a homozygous loss-of-function mutation of GM3 synthase. *Nat Genet* 2004;**36**:1225–9.

11. Wang AS, Kilbane C. Dystonia due to GM3 synthase deficiency. *Mov Disord Clin Pract* 2022;**9**:236–9.

12. Fragaki K, Ait-El-Mkadem S, Chaussenot A. *et al.* Refractory epilepsy and mitochondrial dysfunction due to GM3 synthase deficiency. *Eur J Hum Genet* 2013;**21**:528–34.

13. Gordon-Lipkin E, Cohen JS, Srivastava S. *et al.* ST3GAL5-related disorders: a deficiency in ganglioside metabolism and a genetic cause of intellectual disability and choreoathetosis. *J Child Neurol* 2018;**33**:825–31.

14. Lee JS, Yoo Y, Lim BC. *et al.* GM3 synthase deficiency due to ST3GAL5 variants in two Korean female siblings: masquerading as Rett syndrome-like phenotype. *Am J Med Genet A* 2016;**170**:2200–5.

15. Rudy N, Aoki K, Ananth A. *et al.* Compound heterozygous variants within two conserved sialyltransferase motifs of ST3GAL5 cause GM3 synthase deficiency. *JIMD Rep* 2023;**64**:138–45.

16. Li TA, Schnaar RL. Congenital disorders of ganglioside biosynthesis. *Progress in Molecular Biology and Translational Science*. 2018;**156**:63–82.

17. Bouchon B, Portoukalian J. Purification of the peracetylated glycosphingolipids of the gala series (galactosyl- and galabiosylceramides). *J Chromatogr* 1985;**342**:385–92.

18. Bouchon B, Portoukalian J, Bornet H. Sex-specific difference of the galabiosylceramide level in the glycosphingolipids of human thyroid. *Biochim Biophys Acta* 1985;**836**:143–52.

19. Chatterjee S, Khullar M, Shi WY. Digalactosylceramide is the receptor for staphylococcal enterotoxin-B in human kidney proximal tubular cells. *Glycobiology* 1995;**5**:327–33.

20. Jennemann R, Felding-Habermann B, Geyer R. *et al.* Carbohydrate analysis of chicken heart glycolipids. *Arch Biochem Biophys* 1987;**258**:240–7.

21. Karlsson KA, Larson G. Molecular characterization of cell surface antigens of fetal tissue. Detailed analysis of glycosphingolipids of meconium of a human O Le(a–b+) secretor. *J Biol Chem* 1981;**256**:3512–24.

22. Klock JC, D'Angona JL, Macher BA. Chemical characterization of neutral glycolipids in the human myeloid leukemias. *J Lipid Res* 1981;**22**:1079–83.

23. Macher BA, Klock JC, Fukuda MN. *et al.* Isolation and structural characterization of human lymphocyte and neutrophil gangliosides. *J Biol Chem* 1981;**256**:1968–74.

24. Brown DA, London E. Structure of detergent-resistant membrane domains: does phase separation occur in biological membranes? *Biochem Biophys Res Commun* 1997;**240**:1–7.

25. Brown DA, Rose JK. Sorting of GPI-anchored proteins to glycolipid-enriched membrane subdomains during transport to the apical cell surface. *Cell* 1992;**68**:533–44.

26. Sandhoff K, Kolter T. Biosynthesis and degradation of mammalian glycosphingolipids. *Philos Trans R Soc Lond Ser B Biol Sci* 2003;**358**:847–61.

27. Simons K, Ikonen E. Functional rafts in cell membranes. *Nature* 1997;**387**:569–72.

28. Mbua NE, Li X, Flanagan-Steet HR. *et al.* Selective Exo-Enzymatic Labeling of N-glycans on the surface of living cells by recombinant ST6Gal I. *Angew Chem Int Ed* 2013;**52**:13012–5.

29. Sun T, Yu S-H, Zhao P. *et al.* One-step Selective Exoenzymatic Labeling (SEEL) strategy for the biotinylation and identification of glycoproteins of living cells. *J Am Chem Soc* 2016;**138**:11575–82.

30. Miljan EA, Meuillet EJ, Mania-Farnell B. *et al.* Interaction of the extracellular domain of the epidermal growth factor receptor with gangliosides. *J Biol Chem* 2002;**277**:10108–13.

31. Shih A, Telesco S, Radhakrishnan R. Analysis of somatic mutations in cancer: molecular mechanisms of activation in the ErbB family of receptor tyrosine kinases. *Cancer* 2011;**3**:1195–231.

32. Black LE, Longo JF, Carroll SL. Mechanisms of receptor tyrosine-protein kinase ErbB-3 (ERBB3) action in human neoplasia. *Am J Pathol* 2019;**189**:1898–912.

33. Steinkamp MP, Low-Nam ST, Yang S. *et al.* erbB3 is an active tyrosine kinase capable of homo- and heterointeractions. *Mol Cell Biol* 2014;**34**:965–77.

34. Wee P, Wang Z. Epidermal growth factor receptor cell proliferation signaling pathways. *Cancers (Basel)* 2017;**9**:52.

35. Holbro T, Beerli RR, Maurer F. *et al.* The ErbB2/ErbB3 heterodimer functions as an oncogenic unit: ErbB2 requires ErbB3 to drive breast tumor cell proliferation. *Proc Natl Acad Sci* 2003;**100**:8933–8.

36. Rukazenkov Y, Speake G, Marshall G. *et al.* Epidermal growth factor receptor tyrosine kinase inhibitors: similar but different? *Anti-Cancer Drugs* 2009;**20**:856–66.

37. Hart GW. Nutrient regulation of signaling and transcription. *J Biol Chem* 2019;**294**:2211–31.

38. Yoshikawa M, Go S, Suzuki S-I. *et al.* Ganglioside GM3 is essential for the structural integrity and function of cochlear hair cells. *Hum Mol Genet* 2015;**24**:2796–807.

39. Yoshikawa M, Go S, Takasaki K. *et al.* Mice lacking ganglioside GM3 synthase exhibit complete hearing loss due to selective degeneration of the organ of Corti. *Proc Natl Acad Sci* 2009;**106**:9483–8.

40. Sandhoff R, Geyer R, Jennemann R. *et al.* Novel class of glycosphingolipids involved in male fertility. *J Biol Chem* 2005;**280**:27310–8.

41. Yamashita T, Wu Y-P, Sandhoff R. *et al.* Interruption of ganglioside synthesis produces central nervous system degeneration and altered axon–glial interactions. *Proc Natl Acad Sci U S A* 2005;**102**:2725–30.

42. Collins BE, Ito H, Sawada N. *et al.* Enhanced binding of the neural Siglecs, myelin-associated glycoprotein and Schwann cell myelin protein, to Chol-1 (α-series) gangliosides and novel sulfated Chol-1 analogs. *J Biol Chem* 1999;**274**:37637–43.

43. Capolupo L, Khven I, Lederer AR. *et al.* Sphingolipids control dermal fibroblast heterogeneity. *Science* 2022;**376**:eabh1623.

44. Russo D, Della Ragione F, Rizzo R. *et al.* Glycosphingolipid metabolic reprogramming drives neural differentiation. *EMBO J* 2018;**37**:e97674.

45. Aoki K, Heaps AD, Strauss KA. *et al.* Mass spectrometric quantification of plasma glycosphingolipids in human GM3 ganglioside deficiency. *Clin Mass Spectrom* 2019;**14**:106–14.

46. Bremer EG, Hakomori S, Bowen-Pope DF. *et al.* Ganglioside-mediated modulation of cell growth, growth factor binding, and receptor phosphorylation. *J Biol Chem* 1984;**259**:6818–25.

47. Bremer EG, Schlessinger J, Hakomori S. Ganglioside-mediated modulation of cell growth. Specific effects of GM3 on tyrosine phosphorylation of the epidermal growth factor receptor. *J Biol Chem* 1986;**261**:2434–40.

48. Laine RA, Hakomori S. Incorporation of exogenous glycosphingolipids in plasma membranes of cultured hamster cells and concurrent change of growth behavior. *Biochem Biophys Res Commun* 1973;**54**:1039–45.

49. Wang X-Q, Sun P, Paller AS. Ganglioside GM3 blocks the activation of epidermal growth factor receptor induced by integrin at specific tyrosine sites. *J Biol Chem* 2003;**278**:48770–8.

50. Jiang M, Yu S, Yu Z. *et al*. XBP1 (X-box-binding Protein-1)-dependent O-GlcNAcylation is neuroprotective in ischemic stroke in Young mice and its impairment in aged mice is rescued by Thiamet-G. *Stroke* 2017;**48**:1646–54.

51. Yuzwa SA, Macauley MS, Heinonen JE. *et al*. A potent mechanism-inspired O-GlcNAcase inhibitor that blocks phosphorylation of tau in vivo. *Nat Chem Biol* 2008;**4**:483–90.

52. Huang YF, Aoki K, Akase S. *et al*. Global mapping of glycosylation pathways in human-derived cells. *Dev Cell* 2021;**56**:1195–1209.e7.

53. Si-Tayeb K, Noto FK, Sepac A. *et al*. Generation of human induced pluripotent stem cells by simple transient transfection of plasmid DNA encoding reprogramming factors. *BMC Dev Biol* 2010;**10**:81.

54. Menendez L, Kulik MJ, Page AT. *et al*. Directed differentiation of human pluripotent cells to neural crest stem cells. *Nat Protoc* 2013;**8**:203–12.

55. Cederquist GY, Tchieu J, Callahan SJ. *et al*. A multiplex human pluripotent stem cell platform defines molecular and functional subclasses of autism-related genes. *Cell Stem Cell* 2020;**27**:35–49.e6.

56. Aoki K, Perlman M, Lim JM. *et al*. Dynamic developmental elaboration of N-linked glycan complexity in the *Drosophila melanogaster* embryo. *J Biol Chem* 2007;**282**:9127–42.

57. Nimrichter L, Burdick MM, Aoki K. *et al*. E-selectin receptors on human leukocytes. *Blood* 2008;**112**:3744–52.

58. Anumula KR, Taylor PB. A comprehensive procedure for preparation of partially methylated alditol acetates from glycoprotein carbohydrates. *Anal Biochem* 1992;**203**:101–8.

59. Vukelić Ž, Zamfir AD, Bindila L. *et al*. Screening and sequencing of complex sialylated and sulfated glycosphingolipid mixtures by negative ion electrospray Fourier transform ion cyclotron resonance mass spectrometry. *J Am Soc Mass Spectrom* 2005;**16**:571–80.

60. Mehta N, Porterfield M, Struwe WB. *et al*. Mass spectrometric quantification of N-linked glycans by reference to exogenous standards. *J Proteome Res* 2016;**15**:2969–80.

61. Varki A, Cummings RD, Aebi M. *et al*. Symbol nomenclature for graphical representations of glycans. *Glycobiology* 2015;**25**:1323–4.

62. Wells L, Hart GW, Athens Guidelines for the Publication of Glycomics, D. Glycomics: building upon proteomics to advance glycosciences. *Mol Cell Proteomics* 2013;**12**:833–5.

63. York WS, Agravat S, Aoki-Kinoshita KF. *et al*. MIRAGE: the minimum information required for a glycomics experiment. *Glycobiology* 2014;**24**:402–6.

64. Rojas-Macias MA, Mariethoz J, Andersson P. *et al*. Towards a standardized bioinformatics infrastructure for N- and O-glycomics. *Nat Commun* 2019;**10**:3275.

65. Meng L, Forouhar F, Thieker D. *et al*. Enzymatic basis for N-glycan sialylation: structure of rat α2,6-sialyltransferase (ST6GAL1) reveals conserved and unique features for glycan sialylation. *J Biol Chem* 2013;**288**:34680–98.